TRIBHUVAN UNIVERSITY

INSTITUTE OF ENGINEERING

PULCHOWK CAMPUS

THESIS NO.: M-328-MSREE-2018-2020

Numerical Modelling of Deterioration of Efficiency of Pelton Turbine due to Bucket Erosion

by

Anil Kumar Pachhain

A THESIS

SUBMITTED TO DEPARTMENT OF MECHANICAL AND AEROSPACE ENGINEERING IN PARTIAL FULFILLMENT OF THE REQUIREMENT FOR THE DEGREE OF MASTER OF SCIENCE IN RENEWABLE ENERGY ENGINEERING

DEPARTMENT OF MECHANICAL AND AEROSPACE ENGINEERING

LALITPUR, NEPAL

JULY, 2020

TRIBHUVAN UNIVERSITY

INSTITUTE OF ENGINEERING

PULCHOWK CAMPUS

THESIS NO.: M-328-MSREE-2018-2020

Numerical Modelling of Deterioration of Efficiency of Pelton Turbine due to Bucket Erosion

by

Anil Kumar Pachhain

A THESIS

SUBMITTED TO DEPARTMENT OF MECHANICAL AND AEROSPACE ENGINEERING IN PARTIAL FULFILLMENT OF THE REQUIREMENT FOR THE DEGREE OF MASTER OF SCIENCE IN RENEWABLE ENERGY ENGINEERING

DEPARTMENT OF MECHANICAL AND AEROSPACE ENGINEERING

LALITPUR, NEPAL

JULY, 2020

COPYRIGHT

TRIBHUVAN UNIVERSITY

INSTITUTE OF ENGINEERING

PULCHOWK CAMPUS

DEPARTMENT OF MECHANICAL AND AERO SPACE ENGINEERING

The undersigned certify that they have read, and recommended to the Institute of Engineering for acceptance, a dissertation entitled **" Numerical modelling of deterioration of efficiency of Pelton turbine due to bucket erosion"** submitted by Anil Kumar Pachhain in partial fulfillment of the requirements for the degree of Master in Renewable Energy Engineering.

_____

Supervisor, Prof. Dr. Tri Ratna Bajracharaya

Department of Mechanical and Aerospace Engineering, Pulchowk Campus

_____

External Examiner, Prof. Dr. Bhola Thapa

Department of Mechanical Engineering, Kathmandu University

_____

Committee Chairperson, Dr. Nawraj Bhattarai

Head, Department of Mechanical and Aerospace Engineering, Pulchowk Campus

Date: 29th July, 2020

ABSTRACT

Most of the hydropower plants built in the Himalayan originating rivers contain an enormous amount of sediment in them with the dominance of hard minerals. These hard minerals in the sediment is the major reason for hydro-abrasive erosion of hydro-mechanical and turbine components Erosion depends on many factors and main factors that causes erosion in hydraulic turbines are particle velocity, impact angle, physical and chemical properties and operating conditions. Pelton turbine is used for high head and low flow rate hydropower plants. It is found that in Pelton turbine effect of sediment erosion mainly occurs on the buckets depth and splitter, injectors and needle. The erosion causes mass loss of turbine materials which leads to loss of efficiency and eventually mechanical failure. In this study base on the numerical modelling of Pelton turbine, using a commercial computational fluid dynamics (CFD) code, to analyze erosion in a micro Pelton turbine (2 kW) is analyzed. The validation and comparison of this thesis is done with previously carried out research work in Mechanical Department of Pulchowk campus. The flow modelling has been done with Shear Stress Transport (SST) turbulence model with interphase transfer method as a free surface and mixture model and erosion modelling were done with Tabakoff and Grand erosion model in ANSYS CFX. From the numerical analysis it was found that the erosion rate density due to sediment particle is maximum at bucket splitter and depth. The back side of bucket and tip are also erosion prone area. The result obtained from numerical analysis was compared with experiment to validate the findings, mass loss has been evaluated from the computed erosion rate density. The flow pattern in the Pelton turbine bucket has been numerically modeled for both transient and steady-state case and pressure contour and power has been calculated. The maximum pressure has been found to be $1.34*10^5$ Pa. The sand concentration and the flow rate are the strong parameters for mass loss of the Pelton buckets, its variation has been found to be almost linear. From the numerical analysis, mass loss in each bucket due to sediment particle has been found to be 82 mg for 4 l/s and particle concentration of 261 ppm by considering 72 operating hours. The deviation from the experimental value has been below 20%. From the numerical modelling, the efficiency of Pelton Turbine has been found 69% and this value decreases by 6% and 4% in analytical and experimental results respectively due to the erosion which elucidates the error of 3% as compared to the experimental results.

ACKNOWLEGDEMENT

TABLE OF CONTENTS

LIST OF FIGURES

LIST OF TABLES

LIST OF SYMBOLS

B	Bucket Width, m
B_h	Brinell's hardness number
c	Absolute velocity, m/s
d	Nozzle diameter, m
d_s	Jet diameter
D	Runner diameter, m
E	Specific hydraulic energy, J/kg
f	Bucket frequency, s^{-1}
$f(\gamma)$	Dimensionless function of the
g	Acceleration due to gravity, m/s^2
H	Net head, m
k	Turbulence kinetic energy kg/Nm
n	Rotational speed of runner, rpm
N	Speed of wheel, Rpm
P	Power, kW
Q	Flow rate, m^3 /s
u	Peripheral velocity, m/s
t	Time, s
V	Velocity of jet, m/s
v_f	Volume fraction
v	Relative particle velocity, m/s
w	Relative velocity, m/s
Z	Number of bucket

Greek Symbol

η_h	Efficiency

ω	Angular velocity, rad/s^{-1} Φ
π	Constant
τ	Torque, Nm
ρ	Density, kg/m^3
γ	Impact angle ,rad

LIST OF ACRONYMS AND ABBREVIATIONS

3D	Three Dimension
CFD	Computational Fluid Dynamics
CPU	Central processing unit
DNS	Direct Numerical Simulation method
HPP	Hydropower Plant
LES	Large Eddy Simulation method
NEA	Nepal Electricity Authority
NTNU	Norwegian University of Science and Technology
PPM	Parts per million
RANS	Reynolds Averaged Navier Stoke
RMS	Root Mean Square
RoR	Run- of -River
RPM	Revolution Per minute
SST	Shear Stress Transport

CHAPTER ONE: INTRODUCTION

1.1 Background

Nepal is gifted with huge water resources due to many snow mountains and glaciers in the Himalayas. There are around 6,000 rivers in Nepal. The geographical conditions and huge water resources have made Nepal rich in hydropower potential. The total feasible -potential production capacity is 83,000 megawatts (MW) and an economically feasible production of about 43,000 MW. The technical and economical study carried out by (MWR, 2003) shows that nearly 22,300 MW hydropower capacity is identified for development in the future. But till date, only about 1,182.215 MW is produced (NEA, 2019), which is about 5.3 % of the techno-economically feasible hydropower.

Operating together, it can be summed from the Table 1.1 that 151.24 MW of power is being contributed by the power plants with Pelton turbine to the national grid. Hence, it can be seen that 12.79 % of total power is contributed by Pelton turbine. Furthermore, in Nepal, most of the micro and mini (<1000 kW) employ Pelton turbine for its cost-effectiveness and flat efficiency curve (Panthee et al., 2014). Thus, it clearly illustrates the importance of the Pelton turbines in Nepal. Table 1.2 presents the list of major hydropower projects in which Pelton turbines are installed in Nepal.

Furthermore, there is a large potential for hydropower development in Himalayan region in general. However, there are many technical challenges for hydropower development because of the problem of sediment erosion. The main cause of sedimentation and erosion problems are climatic and physical condition such as tropical climate, immature geology, and intense seasonal rainfall. Therefore, the rivers in this region transport substantial amount of sediments during the monsoon and heavy flood season. The management of the hydropower projects for achieving higher efficiency of hydraulic turbines could be a crucial factor. Hence, this problem has become primary concern for the security, reliability and long life of the hydropower projects. Himalayan rivers consist of large amount of sediment in the form of hard abrasive mineral or rock fragments mainly in the form of quartz. The main cause of sediment particle in rivers is due to the presence of weak rocks of mountain, extreme relief and very high monsoon rainfall. Hence, sediment management has become one of the primary important factors for the safety, reliability and life of infrastructures such as electro mechanical components of hydropower projects.

14

Table 1.1: Major Hydropower Projects with Pelton Turbine

	S.N.	Name of the Project	Total Capacity (in MW)	Unit Capacity (in MW)	Status	Reference
Owned by NEA	1	Kulekhani I	60	30.5	Running	NEA, 2017
	2	Ilam (Puwakhola)	6.2	3.1	Running	NEA, 2017
	3	Panauti	2.4	0.8	Running	NEA, 2017
	4	Sundarijal	0.64	0.32	Running	NEA, 2017
Owned by IPPs	1	Khimtikhola	60	12	Running	IPPAN, 2018
	2	Chilime	22	11	Running	IPPAN, 2018
	3	Upper Tamakoshi	456	76	*Under Construction*	IPPAN, 2018
	4	Sanjen	42.5	15	*Under Construction*	IPPAN, 2018
Total Operating (Running)			151.24			

Even with the best sediment trapping system, complete removal of small sediment particle from river is almost impossible and uneconomical. Due to this reason, most of the electro-mechanical components, mainly turbines in the Himalayan Rivers are exposed to sand-laden water which is subjected to erosion, causing reduction in efficiency and the life of the turbine (Naidu, 1999). Reservoirs lose their storage capacity because of accumulation of sand. Erosion occurs in a wide section of hydraulic machinery (Thapa, 2004). Such erosion depends on eroding particles, velocity size, shape, hardness, chemical properties, surface hardness, operating conditions and impingement angle (S., 2000, Thapa, 2004).

The Pelton turbine is used for high and low flow rate. Being an impulse type turbine, the energy harness in the turbine takes place in two stages, first the conversion of the Potential Energy of the water into Kinetic Energy and secondly the high speed jet striking the runner imparting its Kinetic Energy to the rotational Kinetic Energy of the

runner. Nozzle-Needle, Runner and Casing are the major parts of the Pelton turbine. These parts are the parts of water flow channel and hence they are exposed to the sediment-laden water. It can be expected to see hydro-abrasive erosion in these areas. In Himalayan originating rivers in South-Asia, the influence of heavy rains during the monsoon period (June–September) causes wide variation in river flows. Rainfall is also one of the causes for land erosion and landslides, thus producing high sediment content in the rivers. (M.K. Padhy a, 2011). The presence of hard minerals in the river sediment can be owed to the fragmentation of rock due to chemical and mechanical weathering which is carried by the river during monsoon period. The sediment content in the river is seasonal and is maximum during the monsoon season and minimum during the dry season. (Thapa, 2004; Neopane, 2010).

1.2 Problem Statement

Sediment erosion in the bucket is due to the impact of sand particles on the bucket surface which is commonly understood as solid particle impingement. There are many proposed erosion models for different conditions. But most of the models are co-relational with nature and therefore they are only system-specific. Furthermore, several attempts have been made to reduce the mass loss of material due to erosion. They have been proved to be successful elsewhere, but in the Himalayan region, it is one of the main challenges. Development within the areas of control of sediment from reaching the turbine and protective coating on the surfaces, prone to erosion, are the main areas of research. In the sediment, quartz (60 – 90 %) is dominant mineral which is extremely hard and causes severe erosion damage. Recent advancements in computational techniques and technological advancements have enabled for investigation of flow in Pelton turbine by Computational Fluid Dynamics (CFD) based modelling and predict erosion due to flow. Study of the solid particle impingement within the Pelton turbine bucket has been performed by numerical simulations and result comparison with experimental study can provide better understanding of the mechanisms involved and the best erosion model could be concluded to predict this mechanism. The study and identification of the effect of different shapes and sizes of the sediment particle to predict the erosion rate correctly is a necessity. Therefore, multidisciplinary approach can be used to find the solution sediment erosion problems. More Research and Development is required to find the relation between the particle movement and also the erosion in the turbine bucket.

1.3 Objective

1.3.1 Main objective

The main objective of this thesis is to analyze change in the efficiency of Pelton turbine due to bucket erosion using CFD modelling.

1.3.2 Specific Objectives

- To numerically model flow patterns in Pelton turbine using CFD modelling.
- To perform numerical simulation on Pelton turbine and describe the prediction of the erosion for the bucket.
- To identify critical zones of erosion based upon flow rate and particle concentration.
- To validate the study by comparing the result with the previous findings.

1.4 Assumptions and Limitations

- The occurrence of cavitation in the flow domain is be neglected. Thus, the mass loss is only be due to the impact of sediment particles.
- Water is assumed as an incompressible fluid, hence no change in density is take place. This assumption allow us to use the pressure-based solver on CFX.
- The effect of gravity on the particle motion is small compared with the drag of the carrier fluid flow so that the particles in the bulk phase follow the fluid streamlines. However, near the wall surface, particles deviate from the fluid streamlines and impact on the wall surface.
- The particles maintain their integrity and do not deteriorate.

CHAPTER TWO: LITERATURE REVIEW

Hydropower converts Potential Energy of water into Mechanical Energy via turbine and then to electricity from generator. There are different types of hydro turbines used in power plant when flowing through a turbine on the basis of liquid pressure changes. There are two types of turbines which are Impulse and Reaction turbines.

2.1 The Pelton Turbine

The Pelton turbine is an impulse turbine in which energy of water is converted to Kinetic Energy before it strikes in the runner so there is no pressure difference between the inlet and outlet of the turbine. Therefore, the mechanical energy comes from impulse force of water which is transferred to the shaft from impulse force of jet only. The impulse forces are created in the turbine when bucket is forced to rotate so that the flow vectors change direction which is due to the change in impulse action of Water-jet. The Pelton turbine is suitable when there is low flow rate of water and high head available typically above 200 m (Thapa O. , 2002). The efficiency curve of the Pelton turbine is flat in comparison to the Francis or Kaplan turbine but the peak efficiency is relatively lower. The main reason for this characteristic of the Pelton turbine is because of the multiple number of nozzles (up to 6) which can be used to regulate the flow rate of water. So, for the advantage of Pelton turbine, it could be a very good choice if the available head is unpredictable and changes a lot throughout the season. In small power plants (<10 MW), Pelton turbines are used at heads above 100 m, and are especially suitable when there is no reservoir. (Barstad, 2012). Figure 2.1 depicts the schematic layout and bucket geometry of the Pelton turbine.
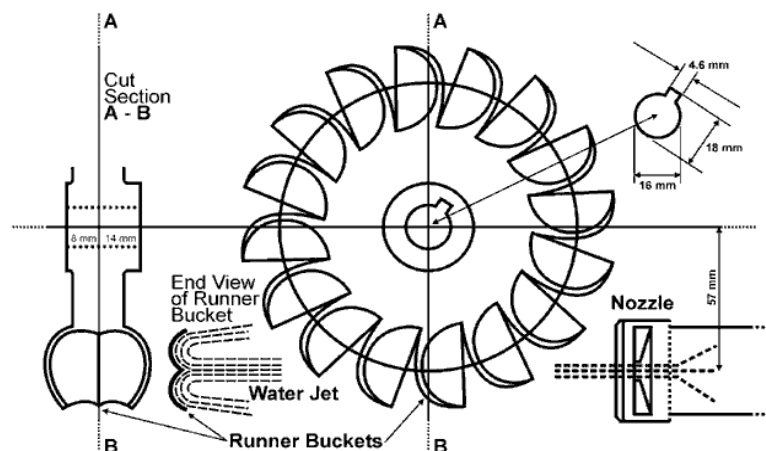
Figure 2.1: Schematic diagram of Pelton Turbine (Miners Foundry, 2016)

2.2 Energy conversion

Figure 2.2 demonstrates the energy conversion in the Pelton turbine. Step 1^* to 1 symbolizes the energy conversion in the nozzle. The flow is taken from a state of high pressure and low velocity, to a state of atmospheric pressure and high velocity. Thus, the energy of the flow is completely converted to kinetic energy relative to the mechanical conversion. In step 1 to 2 almost all the kinetic energy is converted to mechanical energy in the runner. By conducting an energy analysis of a turbo machine runner it can be shown that the specific power E_m transferred from the water to the runner is a function of the absolute and peripheral velocity at the inlet and outlet of the runner:

$$E_m = c_{u1} - u_1 - c_{u2}u_2 \qquad \text{Equation 2.1}$$

Where, c_{u1} and u_1 is the absolute and peripheral velocity respectively. Dividing E_m by the total energy available $E = gH_e$, result in the Euler equation:

$$\eta_h = \frac{E_m}{E} = \frac{c_{u1}u_1 - c_{u2}u_2}{gH_e} \qquad \text{Equation 2.2}$$
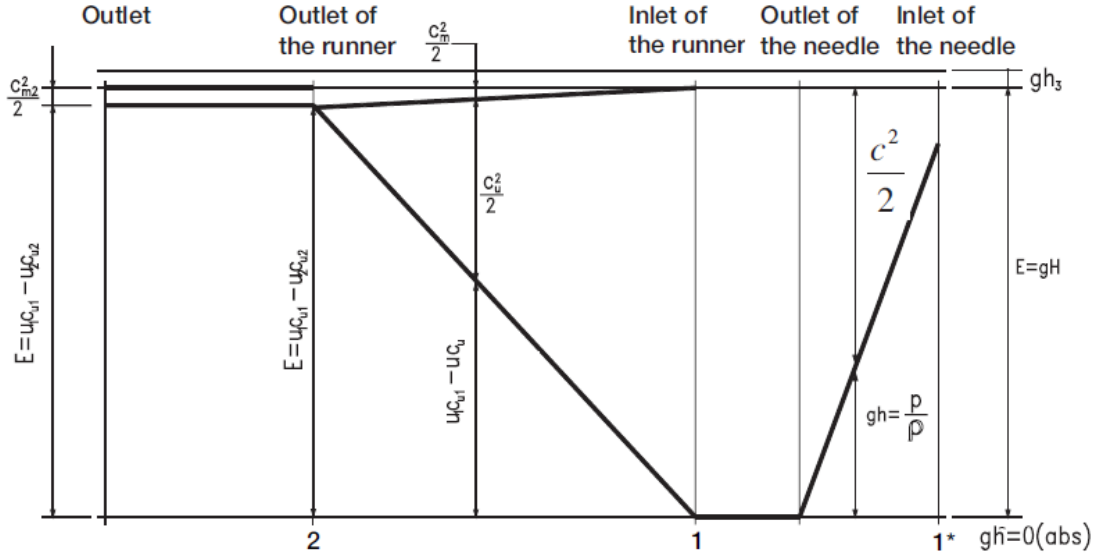
Figure 2.2: Energy conversion in a Pelton turbine runner (Barstad, 2013)

In step 2, the remaining energy can be divided into two components: (1) a small flow velocity $c^2 \, m_2/2$ (relative to the jet) and (2) the potential energy gh_3 of the water relative to the tail-water.

19

2.3 Sand/silt content in Nepal Rivers

The total specific sediment yield of Nepal is around 4240 tons/km^{2}year. For example Marshyangdi and Koshi rivers are highly the sediment laden rives. The study perform in 1981 shows that an average annual load of 26.7 million ton and bed load of 2.9 million tons. (Bajracharya, 2008) Out of this total load 90% are transported in the river during the monsoon season from May to October. Similar condition also applied in rest of river. The complete removal of sand particles from river is almost impossible and uneconomical so maximum number of electro mechanical component of hydropower plants mostly turbine components in Himalayan Rivers are exposed to and laden water and subject to erosion of the turbine, causing reduction in efficiency and life of the components.

According to the material handbook, quartz is the most common variety of silica (brady 1979).it occurs mostly in grains or in masses of white or grey color, but often colored due to impurities. The shape of the quartz usually found in hexagonal prism or pyramids. The grains in sand are often less than 1mm, but crystal up to 50mm have been found. The specific gravity is 2.65. Quartz is harder than most minerals, being 7 Moh's, and the crushed material is much used for abrasive purpose (Thapa O. , 2002).

In Nepal, except Kulekhani, all other project RoR and hence all of them have effect of sand erosion. Turbine of most of the RoR were eroded frequently and mostly refurbished by welding and grinding. Some of these turbine are already replaced with new one. Both the Francis and Pelton turbine of the Kulekhani reservoir are relatively less eroded as compared to ROR scheme.

2.4 Solid Particle: sand

Hydropower station operating with sand laden rivers show considerable erosion of turbine. This first result in the decline of efficiency in these unit and secondly reduces the operation time, i.e. the operation interruption needed to provide maintenance service become more frequent. Sediment are found in the form of clay, silt, sand and gravel with specific gravity approximately 2.6 (Neopane, 2010).Sediment particles in the rivers can be divided into bed load and suspended load based on transport of sediment.

The bed load particle travel close to bed by sliding and rolling with very low velocity than water. And suspended load particle are carried away by following water with same velocity as water.

Sediment are made of fragmentation of rock due to chemical and mechanical weathering. Sediments in rivers are mixtures of particles of different sizes as shows in table 2.1.

Table 2.1 Classification river sediment (Lysne et al., 2003)

Particle	Clay	Silt	sand	Gravel	cobbles	boulders
Sizes (mm)	> 0.002	0.002-0.6	0.06-2	2-60	60-250	<250

2.5 Mechanisms of solid particle erosion

In hydraulic machinery erosion is caused by suspended sediment particle the mechanism of solid particle is mainly buy only four solid particle erosion methods which are abrasive erosion, surface fatigue, brittle fracture, and ductile deformation are mainly applicable. Erosion due to solid particle appear as pitting action when the particle collide with the surface. After the Collison kinetic energy is converted to work, which gives deformation of the material. The basic cause of solid particle erosion are the impact angle and particle velocity (Finnie, 1960). The abrasive erosion, is due to particles with low impact angles which rolls in the surface of metallic material, and material is removed by scratching in the surface by that solid particles. Erosion intensity not only depends upon velocity and impact angle, but also particle shape and hardness matters. Particles with sharp edges will leave a long scar in the material.

2.6 Computational Fluid Dynamics

Computational Fluid Dynamics (CFD), is a branch within fluid dynamics where numerical methods and algorithms, are used to solve fluid flow problems that are far too complex to solve analytically. The continuously increasing computational power, memory and storage of computers, have made CFD a fast growing tool in recent decades. Analytical solutions to the Navier-Stokes equations exist for only the simplest of flows under ideal conditions. For real flows, a numerical approach must be adopted whereby the equations are replaced by algebraic approximations that can be solved numerically. A key benefit of CFD, is that a great amount of time and money can be saved concerning experiments. A single analyst equipped with a computer, can replace experiment designing, material costs, measurement equipment, laboratory personnel etc. The purpose of CFD is not to make decisions directly, it works in conjunction with experiments and experience. The results of a CFD analysis should be thoroughly

analyzed and validated before the model is accepted. It is also important to understand that the solution is only an approximation due to de discretization of the continuous world.

2.7 Governing Equations

The governing equations of the CFD are Reynold's Averaged Navier Stoke Equation. The equations that are solved in the software during the simulation are following: (Rajput, 1999) details of the following equations are mentioned in appendix A.

- Conservation of mass (Continuity)
- Conservation of momentum (Newton's second law)
- Conservation of energy (first law of thermodynamics)
- Ideal gas law
- k- conservation equation
- ε- conservation equation

2.8 Turbulence Model

Turbulence modelling is a critical area of any engineer involved in CFD analysis. There are many different approaches so it is important to have solid grounding in this area in order to choose appropriate turbulence model for simulation.

A complete analysis and quantification of turbulence will probably never be achieved, due to its complexity and unpredictability by stability theory.

There are several approaches to tackle with the turbulence flow.

- Direct Numerical Simulation (DNS) method

- Large Eddy Simulation (LES) method

- Reynolds Averaged Navier Stokes (RANS) equation method

There are different turbulence RANS model that are available in ANSYS. Some of them are: (ANSYS Inc., 2017)

- K-epsilon – Two equation model for free shear and non-wall bounded flow behavior. Was the previous industrial standard.

- K-omega – Two equation model for wall bounded flows, not commonly used.

- SST (Shear Stress Transport) – Two equation model blending the free stream advantages of the k-epsilon model with the wall bounded advantages of the k-omega model. This is the new industrial standard and should be the default choice for most applications (leap australia , 2020).

In spite of the availability of variety of turbulence models, SST turbulence model is used as it gives good convergence in both near wall region and region far away from the wall. (Barstad, 2013). Used this model for the CFD analysis of Pelton turbine which provided satisfactory results.

2.9 Erosion Models

Erosion models are very useful for designing of hydraulic turbine components. Individual Solid particle dynamics are commonly used to develop erosion models. Empirical and statistical relations found from experiment and field study are also used however, now days studies are shifting toward numerical modelling and simulations, due to which importance of numerical modellings are increasing day by day (Thapa, 2004). Truscott, 1972, has found that the most often quoted expression for erosion is proportional to (velocity) ^{n}.

Starting with Finnie erosion model (Finnie, 1960) several erosion models are proposed to study about erosion existing in different areas where there is particle led erosion (Oka & Yoshida, 2005)), (McLaury & Wang, 1997) which are also summarized in ANSYS Fluent Theory Guide (ANSYS Inc., 2017). Erosion models and their applications have been reviewed by Lyczkowski & Bouillard 2002, Sinha et al. 2017 and more recently by Javaheri et al. 2018. Following models are so chosen that they are best to predict erosion under the slurry flow.

2.9.1 Finnie and Oka Erosion Model

In the erosion model by Finnie (Finnie, 1960) for nearly all ductile materials which is expressed in equation 2.6.

$$E = kV_p^n f(\gamma)$$ Equation 2.6

Where, E = Dimensionless erosion mass.

K= Model constant

V_p = Particle impact velocity

f (γ) = Dimensionless function of the impact angle γ.

For metals, the value of the exponent is generally in the range 2.3 to 2.5 radians. 2.3.2 (Oka & Yoshida, 2005)

The erosion model given by Oka (Oka and Yoshida, 2005) is expressed in following equation.

$$W E = E_{90}(\frac{V}{V_{ref}})^{k_2} (\frac{d}{d_{ref}})^{k_3} f(\gamma)$$

Equation 2.7

Where, E_{90} = Reference erosion ratio at 90º impact angle,

V = Particle impact velocity,

V_{ref} = Reference velocity,

d and d_{ref} = Particle diameter and particle reference diameter respectively,

k_2 and k_3 = Velocity and diameter exponents respectively

f (γ)= Dimensionless function of the impact angle γ

2.9.2 McLaury Erosion Model

McLaury (McLaury & Wang, 1997) gives an erosion model to predict the erosion rate of solid particles in water. The model is mainly used to simulate erosion rates in slurry erosion. The McLaury erosion rate is determined by

$$E = AV^n f(\gamma); A = FBh^k$$

Equation 2.8

Where, F=Empirical Constant, V=Particle impact velocity, B_h= Brinell's hardness number of wall material, k is a constant that depends on material composing wall.

2.9.3 Tabakoff and Grant Model

Another widely-used model to predict erosive wear was established by Grant and Tabakoff (1973). Similar to the Finnie model, the Grant-Tabakoff model differentiates between the two wear mechanisms cutting and deformation wear for low and high impact angles. In contrast, the Tabakoff and Grant model combines these two mechanisms in only one equation. The advantage when using one equation is the consideration of both wear-mechanisms for intermediate angles of impact. However,

one equation including both mechanisms gets more complex and depends on several more constants accordingly.

In the erosion model of Tabakoff and Grant, the erosion rate E is determined from the following relation (ANSYS Inc., 2017).

$$E = k_1 f(\gamma) V_P^2 \cos^2 \gamma \ [1 - R_t^2] + f(V_{PN}) \qquad \text{Equation 2.9}$$

Where;

$$f(\gamma) = \left[1 + k_2 k_{12} \sin\left(\gamma \frac{\pi/2}{\gamma_0}\right)\right]^2 \qquad \text{Equation 2.10}$$

$$R_T = 1 - k_4 V_P \sin\gamma \ 1 \qquad \text{Equation 2.11}$$

$$f(V_{PN}) = k_3 (V_P \sin\gamma)^4 \qquad \text{Equation 2.12}$$

$$k_2 = \begin{cases} 1.0 & if \ t \leq 2\gamma_0 \\ 0.0 & if \ \gamma > 2\gamma_0 \end{cases} \qquad \text{Equation 2.13}$$

Here, E is the dimensionless mass (mass of eroded wall material divided by the mass of particle) V_P is the particle impact velocity γ is the impact angle in radians between the approaching particle track and the wall, γ_0 being the angle of maximum erosion. k_1, to k_4, k_{12} and γ_0 are model constants and depend on the particle/wall material combination. To make the model more general, the model is rewritten so that all model constants have a dimension of velocity. The following list shows the link between the constants of the original model and those in CFX

Table 2.2: Constants in Tabakoff and Grant erosion model.

Value	Dimensions	CFX-Pre Variable
K_{12}	(dimensionless)	K12 Constant
K_2	(dimensionless)	
V_1	[Velocity]	Reference Velocity 1
V_2	[velocity]	Reference Velocity 2
V_3	[Velocity]	Reference Velocity 3
γ_0	[degree]	Angle of Maximum Erosion

Where,

$$V_1 = 1/\sqrt{k_1}$$

$$V_2 = 1/ (\sqrt[4]{k_3}\ )$$

$$V_2 = 1/ (\sqrt[4]{k_3}\ )$$

$$V_3 = 1/k_4$$

The erosion of a wall due to a particle is computed from the following relation:

$$Erosion\ Rate = E * N * m_P$$

Here, m_p is the mass of the particle and N is its number rate. The overall erosion of the wall is then the sum over all particles. This gives an erosion rate in kg/s, and an erosion rate density variable in the res file and post-processor in $kg/s/m^2$. Note that this erosion rate is only a qualitative guide to erosion, unless precise values for the model constants are known. The factors k_1, k_2, k_3 and k_{12} are empirical constants depending on the used materials and γ_0 is the angle of impact for maximum erosion damage, normally in the range of 20° to 25°.

2.10 Previous Research Work

In Pelton turbine bucket and needle are most affected part due to sediment erosion. The bucket of the Pelton turbine is altered due to the erosion which cause the change in flow pattern and finally reduction of efficiency. The main effect of erosion is that it causes the mass loss in material because of this highly stressed parts of the material strength is reduced. Flow analysis in Pelton bucket is carried out by graphical and numerical methods (Hana, 1999). The acceleration of water particle in radial, axial and mutually perpendicular direction is plotted graphically assuming particles are always normal to the bucket surface (Brekke, 1994). The graphical analysis also revealed that maximum acceleration normal to the bucket surface can reach up to 50000 to 100000 m/s^2. Such a high acceleration separates the particles from streamline. The curvature of the Pelton bucket is very important due to high acceleration.

Bhola Thapa had initiated the erosion sturdy in Nepal by conducting PhD. Thesis on Sediment Erosion in Hydraulic Machinery. He explain erosion mechanism in hydraulic turbine mainly Pelton, Francis and Kaplan. And case study of different hydro power

projects in Nepal is also carried out. He also conducted the experiment to study the erosion mechanism and give the erosion model. He found that sand particles with small diameter travel along with water in the bucket and then strike the outlet edge of the bucket which cause severe erosion around the outlet. The large particles glide inside the bucket only around the splitter and causing erosion around the splitter of bucket. This process is shown in following figure 2.3.
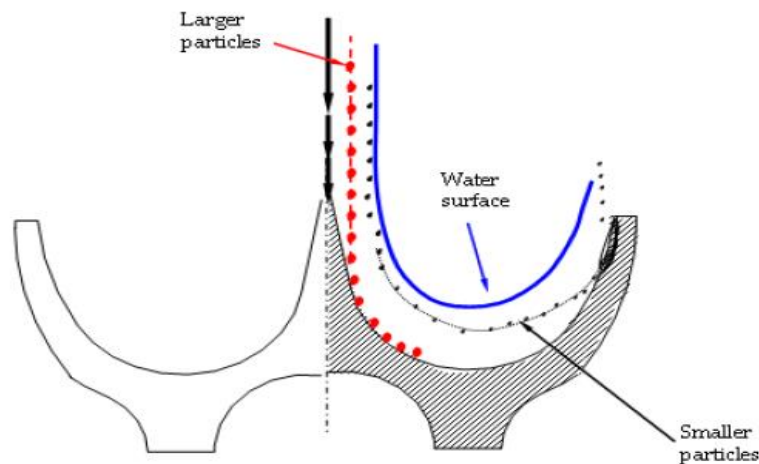
Figure 2.3 Illustration of separation of particle in a Pelton bucket (Thapa and Brekke, 2004)

On the basis of case study of many hydropower plants Thapa and Brekke, 2004, had concluded as following.

• the fine sediment particle cause, erosion on the needle but not much in the buckets

• The coarse sediment particle cause erosion in the buckets and there is less erosion of needles.

• And medium size sediment particles, will cause erosion in both needle and bucket.

Tri Ratna Bajracharaya, faculty of Mechanical department of Pulchowk campus has PhD. thesis on Efficiency Deterioration in Pelton Turbine due to sand-particle-led Bucket erosion. This work is based on experiment and field study of different hydropower of Nepal. Experimental studies conducted have been focus only on a specimen basis not on actual hydropower system. Effect of sand concentration, flow rate and operating hours on bucket erosion has studied and their variation is plotted. He

concluded that sand concentration is the strong parameter for the mass loss of Pelton buckets. The mass loss has been observed mainly on the bucket's splitter. And the mass loss increases with the operating hours for all the values of sand concentrations considered. The effect of sand concentration and operating on the splitter thickness of the buckets is also investigated, it has been observed that the splitter thickness near to the bucket not becomes thicker as a result of blunt occurred due to blunt caused by erosion. Base on the experimental data, a correlation for mass loss as a function of sand concentration and operating hours has been developer by using regression analysis. In order to compare the efficiency of sand effect runner with the original runner value of efficiency has been determined for different values of concentration for different flow rates. It has been found hat efficiency of the turbine decreases with increase in operating hours and the variation is found to be nonlinear. Based on the collected data, a correlation for efficiency as a function of concentration and operating hours has been developed, which predict he value of efficiency (Bajracharya T. , 2007).

Hari Prasad Neopane, Faculty of Engineering Science and Technology, Norwegian University of Science and Technology (NTNU) has performed the analysis in Sediment Erosion in Hydro Turbines. He had conducted the numerical modelling of erosion in Francis turbine using Francis turbine. He analyze the role of operating conditions on erosion rate density demonstrated in simulation analysis. It has been found that erosion process is strongly dependent on the shape of the particle, particle concentration, size of sediment particle and operating flow rate and he concluded that erosion rate can be decreases significantly when it operate at bet efficiency point where as full load operating condition reduces the efficiency and increased turbulence which eventually increases the erosion (Neopane, 2010).

Long scars are also seen in the flow direction in each side of the splitter (figure 2.7 (a) and (b)). Due to direct hitting of sediment particles the splitter and tip of the bucket are most severely damaged part. This surface damage occurred because of hammering action of water jet. The figures 2.7 shown the effect of sediment erosion in different part of Pelton turbine bucket.

a) Bucket surface (Khimti, Nepal)   (b) Splitter, (Rangjung, Bhutan)

c) Splitter and lip   d) lip or cutout of bucket

Figure 2.4: Sediment erosion at Pelton turbine buckets (Neopane, 2010)

Paudel laxman in his PhD. research states that Sand is a naturally occurring material that is composed of fine and divided particles. There is a small difference in sediment and sand, sand is a substance consisting of fine grains of rocks or minerals, usually quartz fragments, found on rivers, beaches, deserts and in soil whereas sediment is a settled matter substance that gets eroded from preexisting rocks and is transported by water, wind, or ice and deposited elsewhere. Sand can be defined as a material made up of grains that are on the range of 0.625 millimeters to 2.0 millimeter in diameter. The common mineral in sand are silica, quartz, mica and feldspar. Sand is a result of different factors including shape, size, composition, severity of weathering conditions, transport distance from its site of origin and physical sorting by wind and or water currents. While Sediments are of different size and its class is defined according to ranges which are composed of organic and inorganic particles of various sizes. Different types of mineral content of sand are quartz, mica, feldspar, silica, clay, chlorites, calcite, dolomite, tourmaline, hornblende, carbonate, phogophite and garnet. Quartz is the most abundant sand mineral content having high stability factor against

29

different atmospheric condition. Quartz is composed of silica i.e. silicon oxide. Mica are widespread and often abundant in both igneous and metamorphic rocks that are fragmented from volcanic rocks. They tend to accumulate with clay, silt, and fine sand. It is crystallize from glass to form a fine-grained mineral matrix. Calcite is another mineral content of sand and its chemical formula is $CaCo_3$. It is white, yellowish and red in color having lustrous of vitreous and pearly. Calcite is best recognized by its relatively low Moh's hardness (3) and its high reactivity with even weak acids, such as vinegar, plus its prominent cleavage in most varieties. Its density is 2.7102(2) g/cm with irregular shape with more than 800 morphologist. Silica constituent of all rock-forming minerals, it is found in a variety of forms, as quartz crystals, massive forming hills, quartz sand (silica sand), sandstone, quartzite, Tripoli, diatomite, flint, opal, chalcedonic forms like agate, onyx etc., and in with numerous other forms depending upon color such as purple quartz (amethyst), smoky quartz, yellow quartz or false topaz (citrine), rose quartz and milky quartz. Feldspar is common mineral content sand found in the crust of earth and is a composite of calcium, sodium and potassium (Poudel, 2016).

Table 2.3 summarize he most relevant literature. It can be seen that quantitative analysis via numerical modelling is least done. Comparison between numerical and experimental can give better understanding the phenomenon which can better predict erosion in the hydraulic turbine.

Table 2.3: Summary of Literature

S.N.	Author(s)	Year	Approach	Majors findings
1.	M. Hana	1999	Computational	Analyse the non-stationary free surface flow in a Pelton turbine bucket.
2.	Bajracharya et.al	2007	Experimental	Experimentally related the erosion and efficiency
3.	L. Kelmetsen	2010	Experimental/ computational	Through experiments the pressure distribution throughout the majority of the flow domain is obtained.
				Use of a dynamic mesh refinement for transient full cycle simulations of rotating Pelton buckets.
4.	Neopane et.al	2011	Review	Erosion in different parts of Pelton turbine are studied. Buckets and needle are highlighted as parts most vulnerable to erosion.
5.	M.K. Padhy et.al	2011	Experimental	Investigate the effect of silt erosion for different silt laden parameters and operating parameters such as silt concentration, size of silt particles
6.	L.F. Barsad	2012	Experimental/ computational	Develop and validate a CFD model that predicts the torque applied to a non-stationary Pelton bucket, subject to a high-speed water jet and correlation of efficiency with silt concentration is found.

7.	Idonis and Aggidis	2015	Review	Numerical modelling of Pelton turbine is summarized
8.	Rai et.al	2017	Field study	Classification of erosion pattern seen in Pelton turbine bucket is done
9.	Zhang et.al	2018	Computational	Three- dimensional numerical simulation of Pelton turbine jet is performed using ANSYS CFX
10.	Sailesh Chitrakar et. al	2018	Review	Various flow phenomena is responsible for particular types of erosion in turbines and their potential consequences is concluded
11.	A.B Timilsina	2019	Experimental/ computational	Sand particle led erosion in Pelton turbine injector

CAPTER THREE: RESEARCH METHODOLOGY

This thesis, being mainly targeted in CFD analysis, requires various steps and methods in sequential order. Such analysis processes are technical and computational, thus it becomes mandatory for the expected results. Methodology of this thesis is based on the numerical modelling of bucket erosion. And adopted methodology are as in Figure 3.1. The study has been commence with the development of 3D Computer Aided Design (CAD) model for modelling the flow domain and the result of sediment sample analysis has been be incorporated to the flow simulation model. The numerical methods and boundary conditions were defined in ANSYS CFX on the basis of the experimental procedure of (Bajracharya T., 2007). Numerical results were validated by comparing with the experimental findings. Both steady state and transient state multiphase flow modelling of the flow domain has been done with ANSYS CFX. Efficiency of the micro Pelton turbine in design condition is obtained from the simulation results were compared with the analytical value. Experimental methodology of (Bajracharya T., 2007) is studied and required data were obtained. Tabakoff erosion model used for the erosion analysis. And result has been compared to that of the experiment value of (Bajracharya T. , 2007).
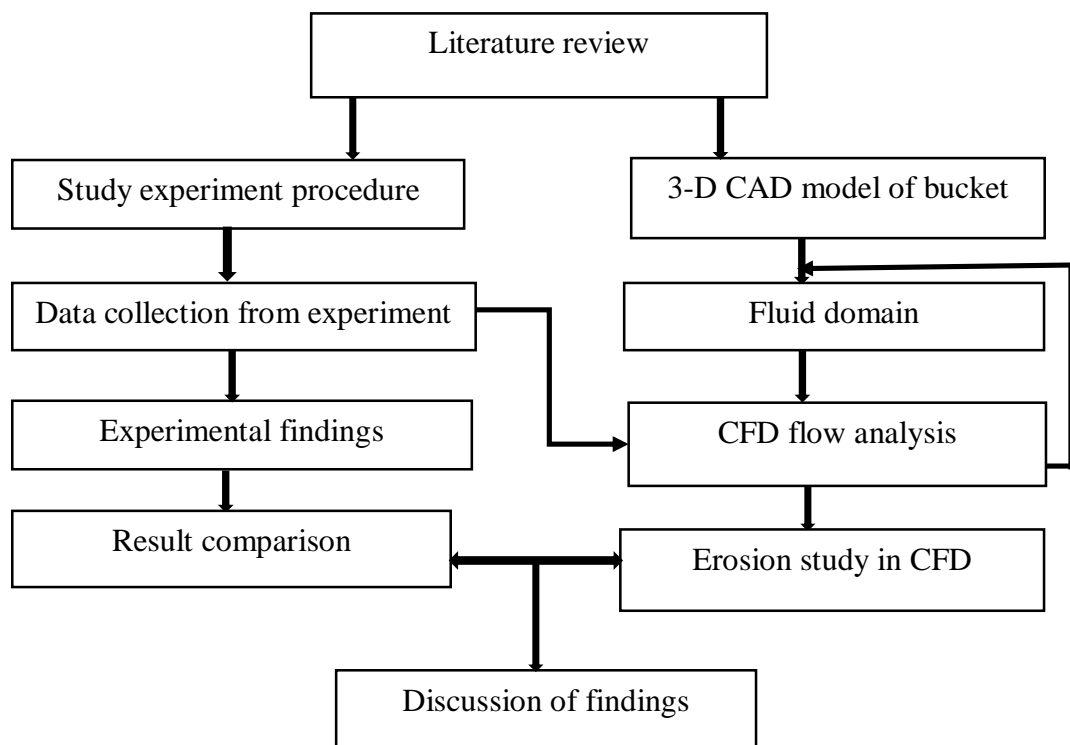
Figure 3.1: Research Methodology

The 3D model of the Pelton turbine has been created with reference to a model turbine at a laboratory test facility as specified in table 3.1. The 3-D model of the bucket is created in CATIA V5. Then the fluid model consists of rotating domain and stationary domain for CFD analysis has been modeled using ANSYS Design Modeler.
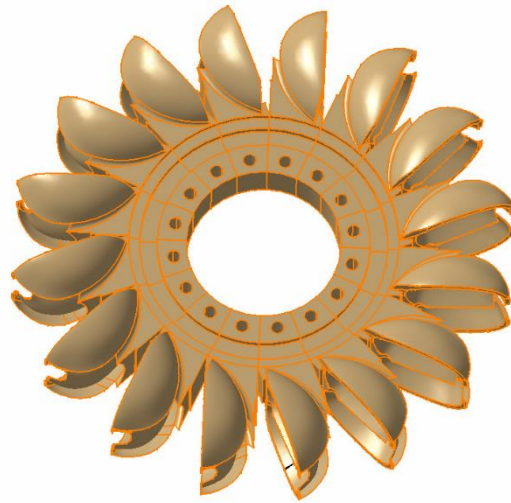
Figure 3.2: 3D model of Micro turbine

Table 3.1: Specification of turbine (Bajracharya T. , 2007)

Type	Pelton Turbine
Manufacturer	Balaju Yantra shala
No. of Bucket	16
Runner PCD	175mm
Maximum power output	2 kW
Net head	47.129 m
Flow rate	5.345 l/s
Turbine rpm	1500 rpm

3.1 3-D domain for ANSYS simulation

The Modeled domain has been created in ANSYS 18.1 own CAD modelling application, DesignModeler. In this thesis, the three-bucket approach is used because the computational cost is a limiting factor and simplicity for the study. Methodology for the 3d domain is shown in figure 3.3.
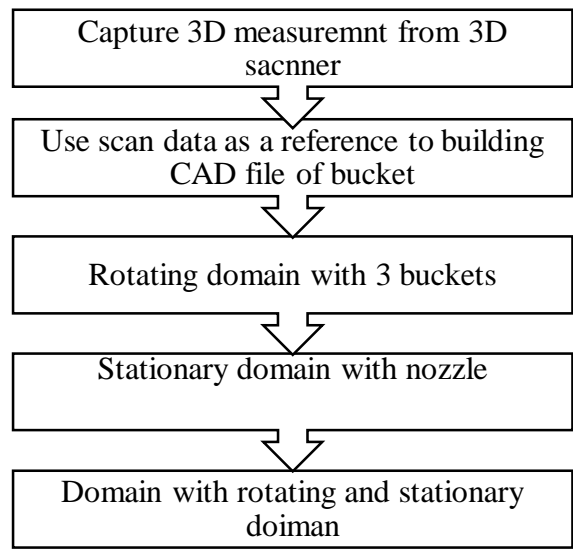
Figure 3.3: Methodology of Domain

3.1.1 Development of CAD model

Pelton Bucket is scanned from 3-D scanner Einscan pro 2x. It does offer an impeccable scanning accuracy of up to 0.02 mm. A Scanned file is then imported in CATIA V5 and the CAD model is created with reference to this original scanned bucket as in figure 3.4.
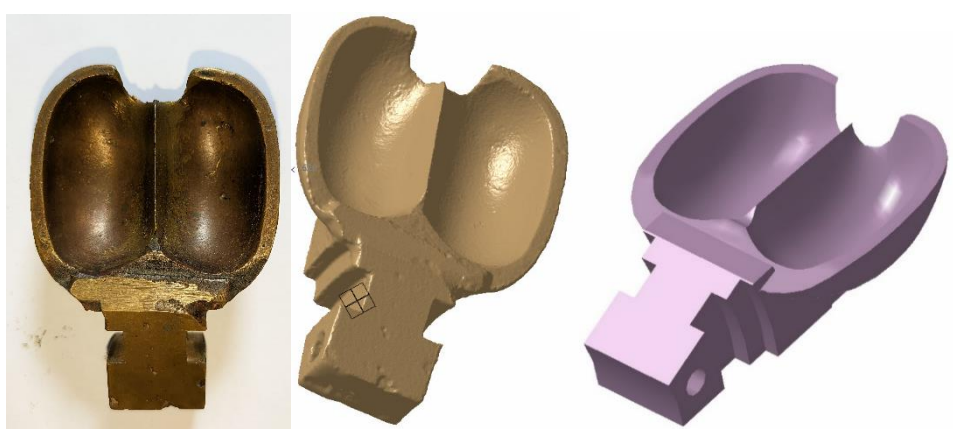
a) Original Bucket   b) Scanned bucket   c) 3-D model from CATIA V5

Figure 3.4: Bucket used for numerical modelling

3.1.2 Physical Model

The physical setup shown in figure 3.5 is a sketch based on a method DynaVec has experimented with (Barstad, 2013). The main concept of this method is that the middle bucket is subject to one, complete water-jet cycle, and data obtained from this bucket can be used to model for the total runner. The domain is defined by the rotating domain,

stationary domain with a nozzle. The Modeled domain has been created in ANSYS 18.1 own CAD modelling application, DesignModeler. The rotating domain consists of three Pelton buckets and the volume this geometry occupies is subtracted from the rotating fluid-domain by using Boolean application. The dimension of both rotating and stationary domain is set at 120º which quarter of a disk with three hollows. Due to the lack of a turbine casing and the injector components the geometry becomes simpler.
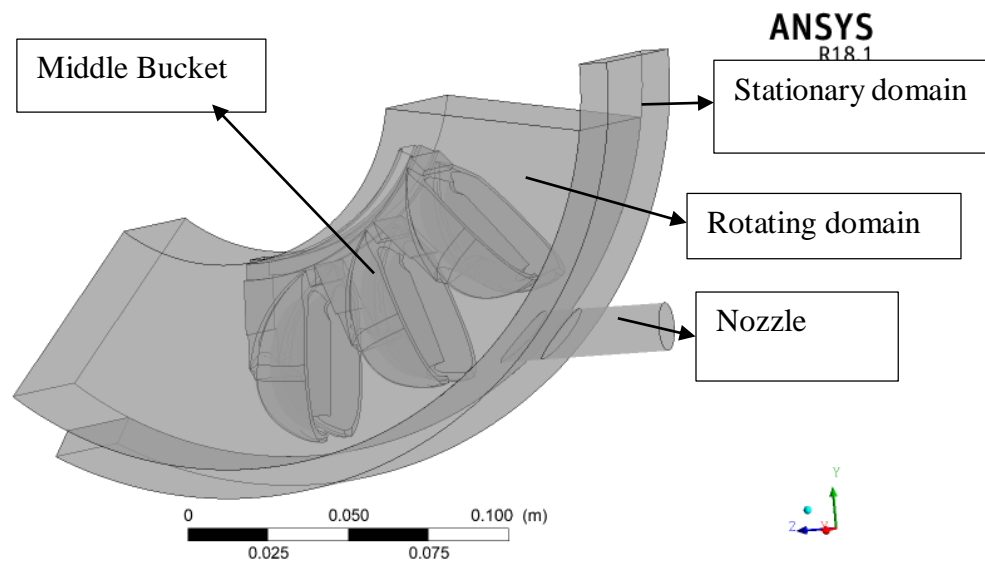
Figure 3.5: Flow domain

The analysis portion consists of a setup of nozzle and Pelton runner arranged in such a way that the jet is fully developed before it strikes the bucket. This portion is bounded by domains, namely stationary domain and rotating domain. The former one includes nozzle setup and latter one includes rotating Pelton wheel. One of the important steps introduced here is truncation of bucket and limiting its number up to three. Since at a time only three of the buckets entangle with water jet giving a full strike at the middle one and partial strike to the other two, the results after the analysis of three buckets applies well to the whole runner. Three buckets were sliced at 22.5º with horizontal axis (T.R. Bajracharya, 2008). The fluid domain has been extended to 120º degree for easier measurement of torque. The torque must be zero at the end of the simulation. The stationary domain has been then created. Nozzle has been made (diameter being coincident with splitter) to make pitch ratio 1

3.2 CFD Solution Procedure

The method adopted for any CFD simulation process is summarized in figure 3.6.

36

```
┌─────────────────────────────────────┐
│            Pre-Processing            │
└─────────────────────────────────────┘
                  ⇓
┌─────────────────────────────────────┐
│              Solution                │
└─────────────────────────────────────┘
                  ⇓
┌─────────────────────────────────────┐
│           Post-Processing            │
└─────────────────────────────────────┘
```

Figure 3.6: Process Flow of CFD Simulation

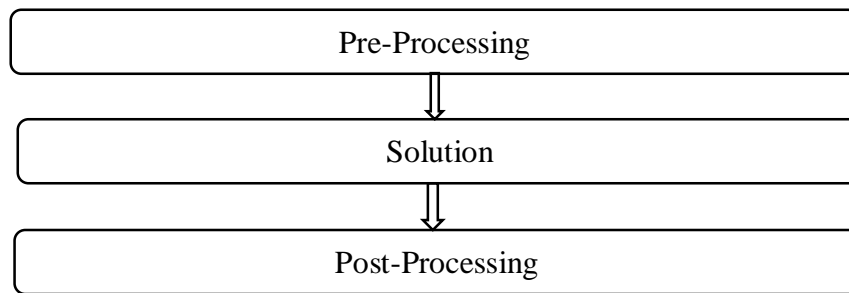1. **Pre-processing**, in which the analyst develops a finite element mesh to divide the subject geometry into subdomains for mathematical analysis and applies material properties and boundary conditions.In this case, to model the flow domain, 3D CAD software, CATIA has been be used for its ability to better model the surface topology. Better modelling of surface topology is expected to ease us during the mesh generation. As three-dimensional flow simulation has been be done and our domain is axisymmetric, a part of the domain has been modeled which has be used to generate the whole domain. The meshing of the domain has been be done by using ANSYS 18.1 meshing. Boundary conditions as well as sand particle information has been be used as per (Bajracharya et al., 2008). With ANSYS CFX, the eroded shape of the bucket has been studied for different flow rate, particle concentration and operating hours. The results has been obtained for different erosion models and the eroded shape has been be compared to the experimental one.

2. **Solution**, Here ANSYS CFX 18.1 has been used for the solution. Fluent is a finite volume-based where as ANSYS CFX solver uses finite elements (cell vertex numeric). Most commercial codes are now finite volume based. The finite volume method is easier to implement for unstructured meshes and is also more stable. Most importantly, CFX can be personalized using UDFs.

3. **Post-processing**, in which the analyst checks the validity of the solution, examines the values of primary quantities (such as displacements and stresses) and derives and examines additional quantities (such as specialized stresses and error indicators). An inbuilt program in ANSYS Workbench CFD Post is used for post-processing the CFD results.

3.2.1 Pre-processing

The meshing of the both rotating and stationary domains have been carried out in ANSYS 18.1 meshing. Fluid domain have been divided in two separate components, one for the stationary domain and one for the rotating domain. The main reason to divide into two standalone component is that rotating domain has been meshed with an advanced size function, while the stationary domain has not used this function.
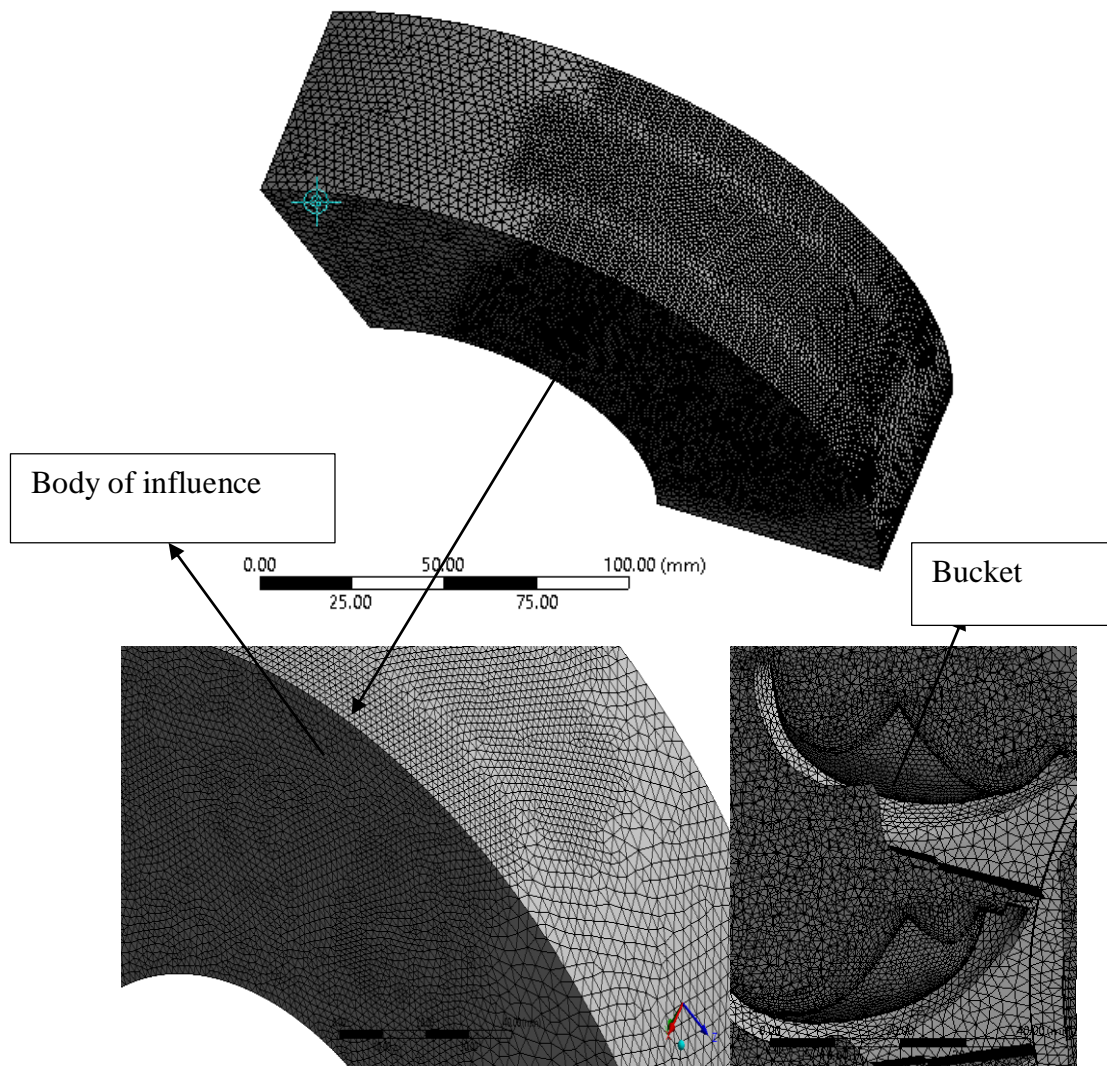
Figure 3.7: Meshing of rotating domain

The rotating domain have been meshed with the advanced size function "Proximity and Curvature" and consists mainly of tetrahedral elements and body of influence is used at water jet inlet and water outlet with fine mesh. The "body of influence" of size 1mm has been used as shown in figure 3.7 to increase the element density in this area.

Fine mesh has been performed in the stationary domain around the jet region with prismatic element of element size of 1 mm and the whole domain consists mostly of

hexahedral elements of maximum size of 3mm. An inflation layer in the radial direction of jet wall region has been used.

Figure 3.8: Meshing of stationary domain

3.2.2 Work flow

CAD modelling of the fluid domain, generation of a computational mesh, physical setup and post-processing has been prepared for the flow simulation and erosion modelling.

Figure 3.9: ANSYS Workbench overview of a simulation

Figure 3.9 depicts the resulting CFD case, ready to run, in ANSYS CFX. This includes the separate domain creation and mesh generation for stationary and rotating components. The physical setup has been performed in ANSYS CFX p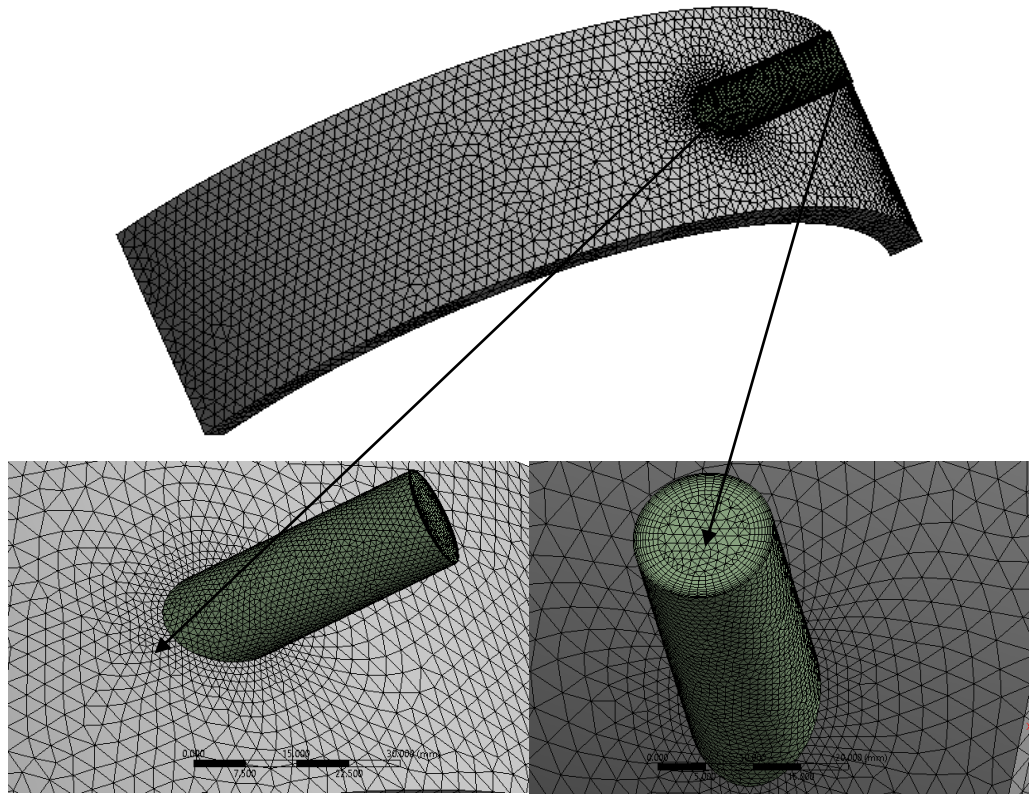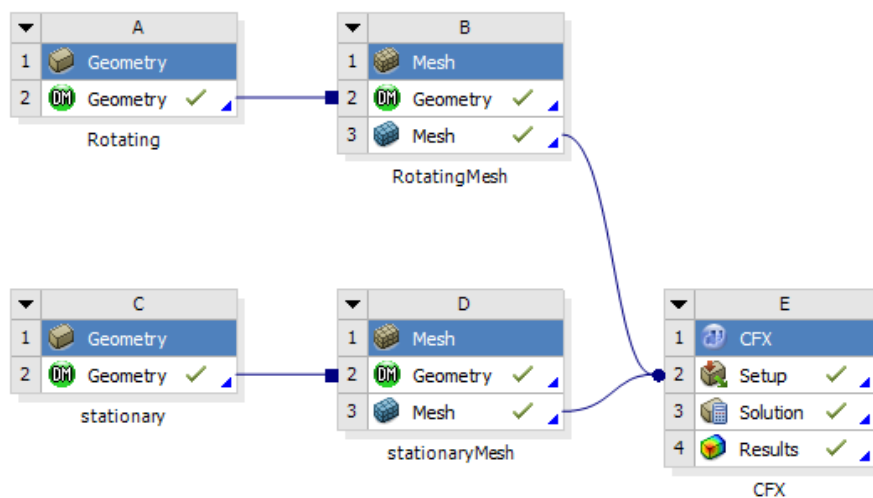reprocessor. The problem has been solved in the solver and the result has been analyzed in the post processing. Two different meshing has been performed for both the domains.

3.2.3 Flow analysis

The flow simulation has been carried out by using available Computational Fluids Dynamics (CFD) code, namely ANSYS CFX. A pre-processor is available in the software to generate the computational grid. In the solution option, basically inlet and boundary conditions, turbulence model, and discretization scheme, are specified on the basis of requirements. The final step in numerical process is by running the flow using solver to generate the actual flow field simulation. The analysis portion consists of a setup of nozzle and Pelton runner arranged in such a way that the jet is fully developed before it strikes the bucket. This portion is bounded by domains, namely stationary domain and rotating domain. The stationary domain includes nozzle setup and rotating domain includes rotating Pelton buckets. One of the important steps introduced here is truncation of bucket and its number is limited up to three. Since at a time, only three of the buckets entangle with water jet giving a full strike at the middle one and partial strike to the other two, the results after the analysis of three buckets apply well to the whole runner.

<u>Transient state</u>

Two fluid domains have been separately created, one for the rotating domain and one for the stationary. There is no pressure difference in Pelton turbine and pressure is atmospheric around the turbine so that the reference pressure in both the domains have been set to 1 atm. This difference has been ignored. In free surface flow, the homogeneous multiphase model should be used when possible (ANSYS Inc., 2017). The flow in Pelton turbine is considered as a drag dominant in the interphase flow because the air relative velocity to water-jet is very low. Due to this property, the flow used in the fluid domain can be used as homogeneous model. But, this model does not apply to droplets falling under gravity in a gas. At the same time, these droplets probably have a high velocity relative to the surrounding air making the gravity force contribution small in comparison. The standard free surface model has been chosen

because the air-water interface can be considered distinct (ANSYS Inc., 2017). The surface tension coefficient has been set manually 0.0728 Nm^{-1} (White, 2006), and the surface tension model Continuum Surface Force with the primary fluid as water has been also chosen. This model is based on the Continuum Surface Force model of Brackbill et al (J.U Brackbill, 1992). In Pelton turbine, there is slightly temperature difference before and after the conversion of energy because friction in the runner is converted into heat but for this analysis heat transfer has been neglected. For initial boundary conditions, the cartesian velocity components has been selected and its value has been set to zero. The volume fraction of air and water has been set to 1 and 0 respectively. The interface model General Connection and the frame change/mixing model Transient Rotor Stator has been chosen. The General Connection model allows the connection of non-matching grids and fully transient sliding interfaces between domains. In this case both interfaces are similar and the simulation is non-periodic, thus the pitch ratio has been set manually to 1. To apply rotation to the rotating domain, Domain Motion in the rotating domain has been set to Rotating, and Angular Velocity has been defined by the expression "angular velocity". In this case, the angular velocity is negative because the domain has been modeled to rotate in the clockwise direction about the X-axis.
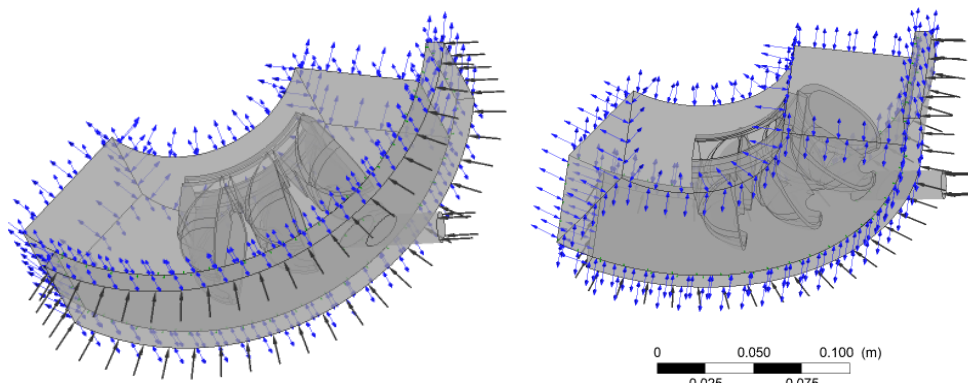
Figure 3.10: Boundary setup

3.3 Solver Control and Output

The default transient scheme, Second Order Backward Euler, has been chosen because it is recommended by ANSYS for most transient runs. The minimum number for coefficient loops has been set to 5 to ensure that at least 5 iterations are completed per time step. According to (ANSYS Inc., 2017), 10 coefficient loops per time step is usually adequate to resolve the strong non-linearities in multiphase flows, thus the

41

maximum number of coefficient loops has been set to 10. The residual level is very important measure for the convergence of simulation because it relates directly to whether or not the equations have to be solved. In this case, the residual type RMS has been chosen with a residual target of 1×10^{-4}.

3.3.1 Steady state

Table 3.2: Over view of basic setup used for all simulation

Solver	ANSYS CFX 18.1
Time discretisation	Transient/steady state
Advection scheme	High resolution
Transient scheme	Second order backward Euler
Turbulence model	SST with automatic wall function
Multiphase model	Homogeneous model std. free surf model
Surface tension model	Continuum surface force
Surface tension coeff.	0.072 Nm^{-1}
Convergence criteria	RMS, residual target $=1*10^{-4}$
Hardware	Processor: Intel(R) core(TM) I5-2450CPU@2.5GHz memory:8 GB

3.3.2 Erosion Modelling

In this Tabakoff and Grand erosion model is selected. The erosion modelling has been carried out in ANSYS CFX. Following steps have be adopted for erosion rate prediction with different models.

1. Flow pattern prediction under different velocities
2. Particle tracking
3. Erosion rate density prediction

In this thesis steady-state analysis is selected because of the less computational time cost. Two phase mixture of water and sediment particle have been considered and for turbulence model Stress Transport (SST) model is selected. It is the two-equation model consists the free stream benefits of the k-ω model and also with the wall bounded

advantages of the k-ε model. SST turbulence model with automatic wall function has been used as good convergence has been required in both near the wall region and region far away from the wall (ANSYS Inc., 2017). Pressure inside the Pelton runner is atmospheric thus reference pressure in both fluid domain have been set at 1 atm. Two fluid domains one for the rotating domain and one for the stationary domain have been created and relative pressure between inlet and outlet has been set 0 atm. Therefore particles have been modeled based on sand analysis which has been carried in an experimental study in 2008. The density of quartz is 2000 kg/m^3 and Molar mass of 1 kg/kmol is used. The diameter of the particle has the minimum for 0.05 mm, maximum for 0.15 mm with an average value of 0.1 mm. Tabakoff and Grand erosion model has been used and fully coupled particle coupling of sediment particle and water is selected (ANSYS Inc., 2017).

The interface model General Connection and the frame change/mixing model Frozen Rotor Stator have been chosen and the pitch ratio has been set manually to 1.To apply a rotation to the rotating domain, Domain Motion in the rotating domain has been set to Rotating with the value of 1500 rpm in the clockwise direction of the x-axis of runner model has been used. The all three buckets have been defined as no slip, smooth walls. Mass flow rate inlet has been defined for the jet with a value of (2- 4) kg/s and particle mass flow rate of (0.001004 - 0.00069) kg/s with reference from the experimental data. No slip, smooth wall near jet region which gives better jet stability (Barstad, 2012). Opening boundary of relative pressure 0 atm. has been defined in other part of the domain. The symmary of boundary condition with appropriate value are present in table 3.3.

Table 3.3: Boundary conditions

Variable	Value
Water density	997 kg/m^3
Sand particle density	2.65 gm/cm^3
Diameter of the particle	62-200 μ
Inlet mass flow rate of water	2-4 kg/s
Reference pressure	1 [atm.]
Inlet mass flow rate of particle	261 ppm/s to 2000 ppm/s

CHAPTER FOUR: RESULTS AND DISCUSSION

4.1 Flow analysis

For validating the fluid domain, flow analysis is an important factor in numerical modelling. In this study, flow analysis of model has been carried out in both transient and steady state. Transient state flow simulation is carried out to validate the model with the design conditions and whereas steady state flow simulation is carried out by taking reference of previously carried out experimental study. Due to the time limitations, mesh independency test has been carried out using steady state flow modelling.

Mesh independency test

Mesh or grid independent study is done in order to get a solution that does not vary significantly even when we refine our mesh further. For the mesh independency test, six different mesh sizes have been tested with an effective head of 40 m. The mesh size on the rotating domain and size of jet region is controlled by element size. The relevance has been increased for finer mesh. Mesh independency test is based on the torque value obtained from steady state simulation result.
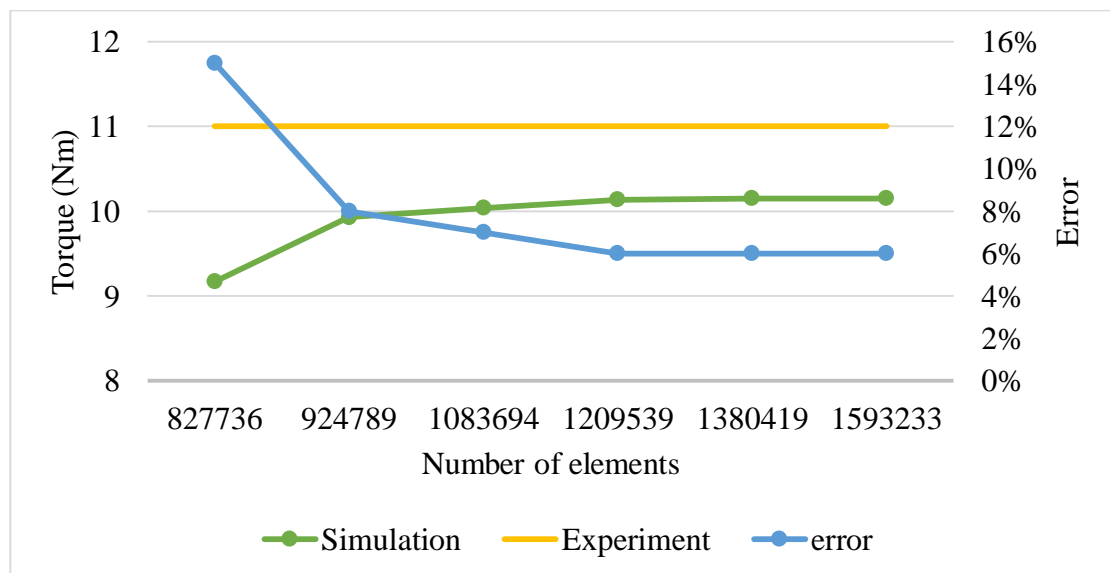

Figure 4.1: Mesh independency test

Each mesh has been created with the same physical setup and boundary conditions. During the simulations, results obtained from simulation have been directly dependent on the accuracy in quality of mesh. And it has been performed while analyzing the torque variation by developing the SST turbulence model. It is observed that, from the

result in figure 4.1 a finer mesh give a solution of a little higher accuracy than coarse mesh, but at the expense of computational power and time. About 1.2 million elements mesh size has been required to obtain mesh independent result. It appears that no significant enhancement is to be expected from a further refinement of the mesh.

4.1.1 Steady state flow modelling

Figure 4.2 shows the steady-state numerical simulation result, based on the two-phase homogeneous model and SST turbulent model. Position of nozzle is placed at the middle bucket. It is clear that, as the water starts entering into the bucket, the inner surface of the middle having some water volume fraction inside it. It indicates that at particular instance of time and runner rotation, more than one buckets are having water volume fraction. The amount of the water flow strikes the bucket splitter sides and back surface of the bucket known as backwash is also visible.This water jet at the back side and other side surface of the bucket create some force to the buckets and if this water fraction is high, then the intensity of force on the bucket could be high and it is acting as a brake on the runner and reduce the strength of the buckets.
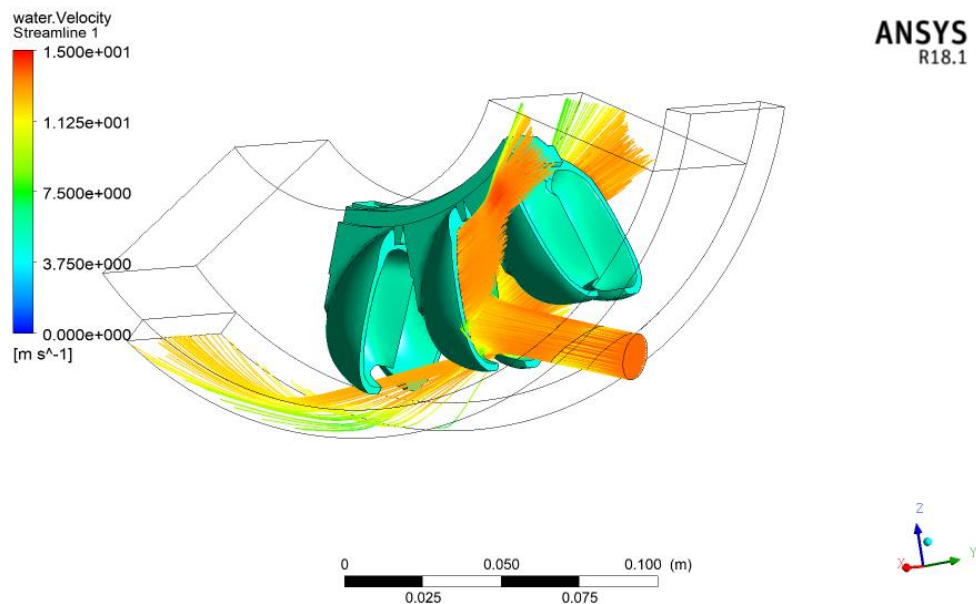

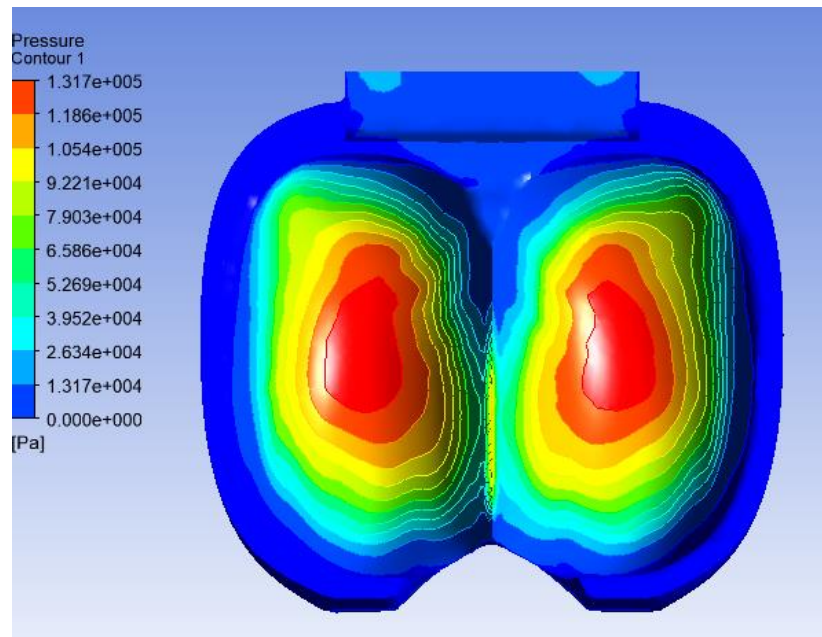Figure 4.2: Streamline flow in Pelton turbine buckets

Figure 4.3: Pressure distribution in the bucket

Figure 4.3 shows the pressure contour of the middle Pelton bucket. From numerical analysis it is found that maximum value of pressure is $1.317 * 10^5$ Pa. And the maximum pressure intensity is seen around pitch circle diameter of Pelton turbine bucket. Pressure at the splitter is has also greater value than other parts of the bucket.

4.1.2 Transient state flow modelling

The transient state simulation differs from steady state mainly by the presence of higher order terms dealing with time in transient state. In transient state these all value are taken into account, hence more accurate results from transient simulation is expected. A visualization of the flow in the turbine buckets for this study can be seen in Figure 4.4. From figures 4.4 it is seen that small amount of water leakage from the bottom bucket with low water-jet velocity. These flow visualizations obtained from simulation result gives good information about the flow pattern inside the bucket. The water jet from the nozzle entered into the Pelton runner, hits the buckets splitter and dividing the water-jet into three parts. From the bottom of the nozzle it, touched the outside and inside part of the top bucket. Then second portion of the water-jet is the one from the middle part of the fluid domain, which hit directly the middle bucket. Lastly, the remaining portion of the water jet is passed into the latter bucket. It is observed that the part of the flow escaping from the cutout of the bucket and the lateral sheet flow.
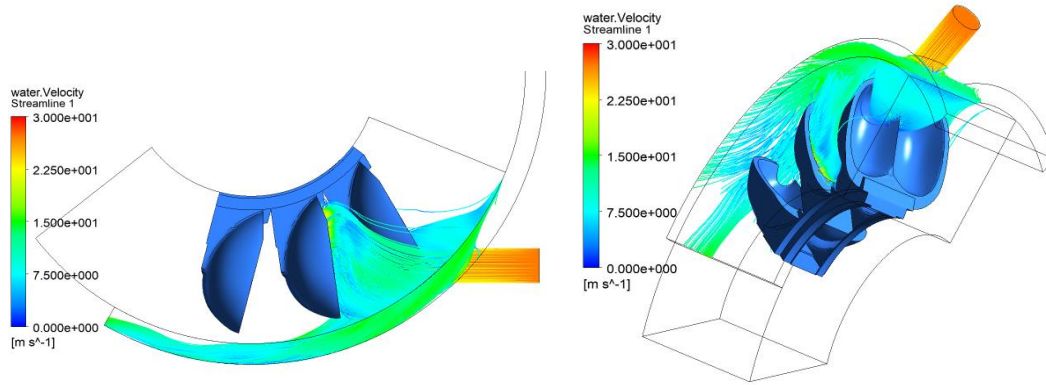
Figure 4.4: Torque generated by middle bucket versus angular position

- **Efficiency calculation**

The total torque curve is shifted by the single blade passage phase for the whole range of total torque values and summed to give the total torque acting on the turbine shaft. The torque generated by the middle bucket is replicated over time to determine total torque generated by Pelton turbine. This is done by assuming that at stable conditions every bucket is producing identical torque periodically. The replication has been done till the summation graph gave steady values which occurs after those describe above quite common and can be found in the literature (Barstad, 2012).
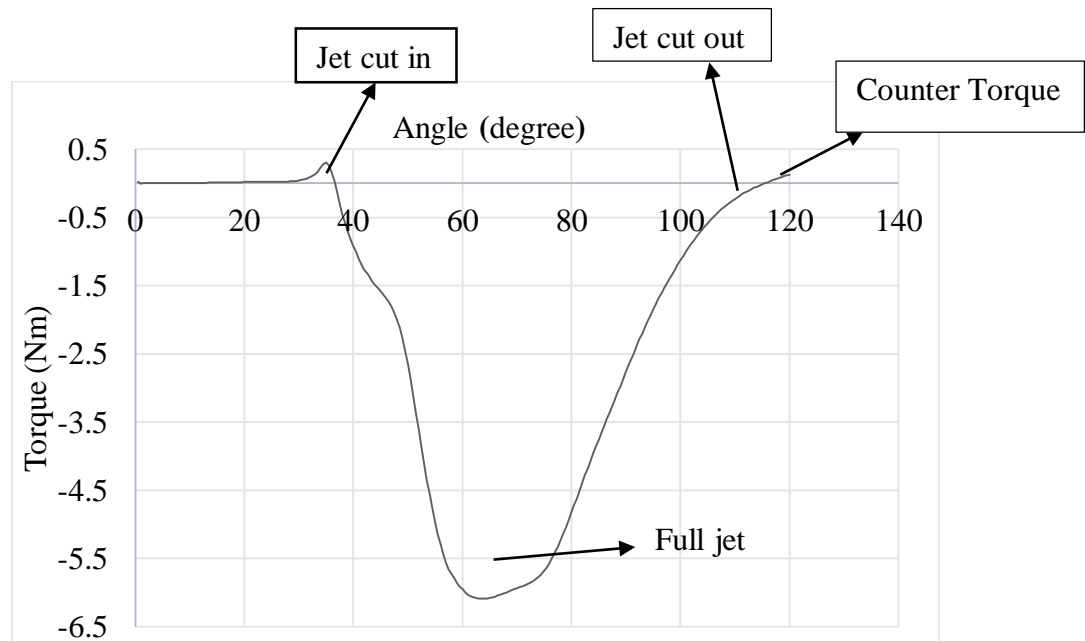

Figure 4.5 : Torque generated by middle bucket versus angular position

The total torque of the runner is calculated by taking reference data obtained from the middle bucket. In principle, this problem is quite simple, but varying time step size due

to the adaptive time steps and point specific bucket frequency $f = wZ/\pi$ complicated this task. To calculate the complete torque on the runner, the torque from a middle bucket as shown in figure 4.5 bucket has been duplicated n times and each duplicate has been shifted $n*1/f$ in time. This imitates n buckets passing the jet (16 buckets). The torque data obtained from the numerical analysis has been processed in MATLAB. The varying time step size lead to some difficulties because the torque measurements for two buckets would not match up when one bucket is shifted $1/f$ [s] in time. To solve this problem a fixed time step size has been calculated so that two time series align when one is shifted $1/f$ [s]. From MATLAB total torque of Pelton runner is found 12.3 Nm. The MATLAB script for the post-processing is found in Appendix E.

To calculate the efficiency of the modeled Pelton runner, power input and output need to be calculated by using equation 4.1 and 4.2 respectively by using two variable: the net pressure head and the flow rate.

$$P_{input} = \rho g Q H_{net} \qquad \text{Equation 4.1}$$

$$P_{out} = \frac{2\Pi NT}{60} \qquad \text{Equation 4.2}$$

The Hydraulic efficiency of the Pelton runner in this model has been calculated by as follows:

$$\eta_h = \frac{P_{out}}{P_{input}} \qquad \text{Equation 4.3}$$

By using equation 4.2, calculated power output from simulation result has been found to be 1.93 kW which is around 10 % less than design power output (2 kW). The torque results obtained from CFD showed that the Pelton turbine has efficiency of 75.21%.

4.2 Sediment sample analysis

Sand is an example of class of materials called granular matter and it is naturally occurring rock consist of particles or granules ranging in size from 0.063 to 2 mm an individual particle in this size is termed a sand grain. The next smaller size class in geology is silt: particle below 0.63 mm down to 0.004 mm in size. The next larger size class above is gravel with particles ranging up to 64mm. in this thesis sand samples is taken on the basis of (Bajracharya T. , 2007). It is found that from the analysis of sediment sample for particle size distribution reveal that the most of the particle (>90%) are less than 1mm diameter as in figure 4.6.
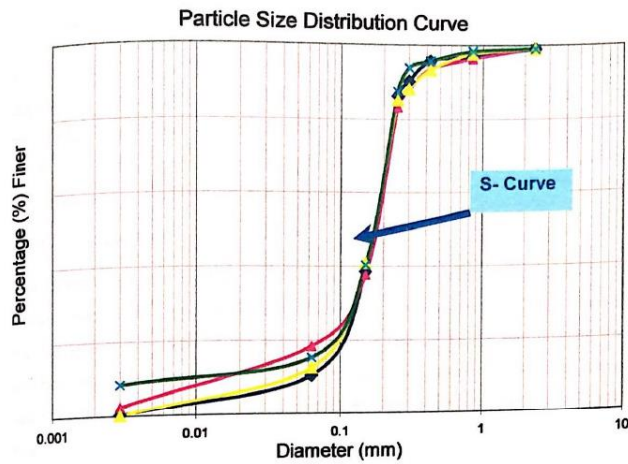
Figure 4.6: S curve development from particle size distribution (Bajracharya T. , 2007)

The mineral composition analysis (see table 4.1) reveals the presence of quartz, feldspar, mica, tourmaline, garnet and clay in sediment sample. Among these quartz is the most abundant mineral with presence average 76% by volume.

Table 4.1: Mineral content analysis (Bajracharya T. , 2007)

Minerals	Percentage(%) by volume				Mohs'	Remarks
	<1m m	<1mm	<1mm	Average%	Hardnes scale	
Quartz	75	76	77	76	7	Mica content is high. Other minerals mainly content garnet, tourmaline and rock fragments
Feldspar	7	6	6	6	6	
Muscovite	5	6	5		2-3	
Biotite	10	9	9	15		
Others	3	3	3	3	>6	

4.3 Numerical study of erosion

An important consideration in these simulations is erosion to the bucket of Pelton turbine due to different flow rate and particles concentration. The effect of particle erosion is expressed by the erosion rate density (kg/s/m^2), which is due to pressure and shear stress due to the flow. In order to visualize erosion predictions in a convenient

manner, predicted erosion data is transferred to a post-processor. This post-processor is used to generate contour plots of predicted erosion quantities. This allows the simultaneous examination of the flow solution, particle trajectories, and erosion predictions and also gives the ability to identify areas of high erosion. This can be seen as coloured spots. Red colour indicates the highest value of erosion intensity, whereas blue colour denotes the lowest intensity of erosion. Figure 4.7 shows the particle tracks and the streamlines from the jet inlet. The black lines are particle tracks and the other coloured lines are streamlines of water. They are distributed uniformly and continuously. This may mainly result from a uniform inlet and small particle diameter which lead to small inertial force than interaction force.
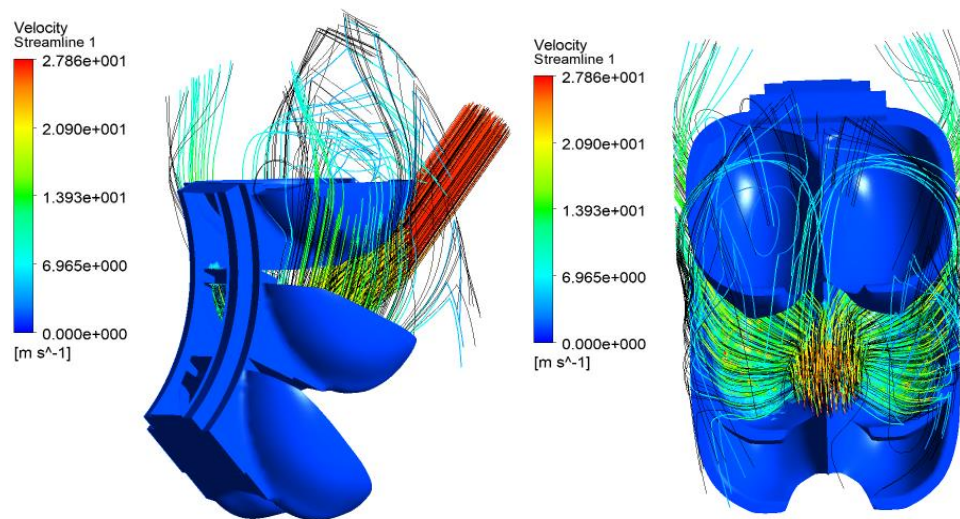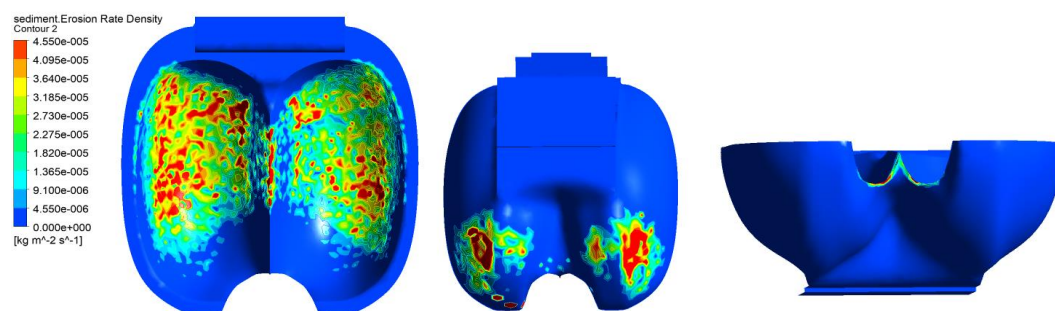

Figure 4.7: Particle track

Figure 4.8 (a), (b) and (c) show the erosion distribution in the bucket. It is found that four possible erosion regions have been detected which are at the splitter, the inside area of bucket, backside and at the tip of the bucket.

(a) Front side of Bucket   (b) Backside of bucket   (c) Lip

Figure 4.8: Erosion pattern different parts of the bucket

4.3.1 Erosion rate calculation

From the experiment, 69 mg mass loss in each bucket has been found at a flow rate of 0.004 m³/s and particle concentration of 261 ppm with 72 operating hours. To convert the erosion rate density obtained from the simulation results to mass loss, three erosion prone areas in the bucket as shown in figure 4.9 have been taken into account. The surface area has been measured by using CATIA V5 and mass loss has been calculated. The calculated value of eroded mass has been found to be around 82.5 mg.
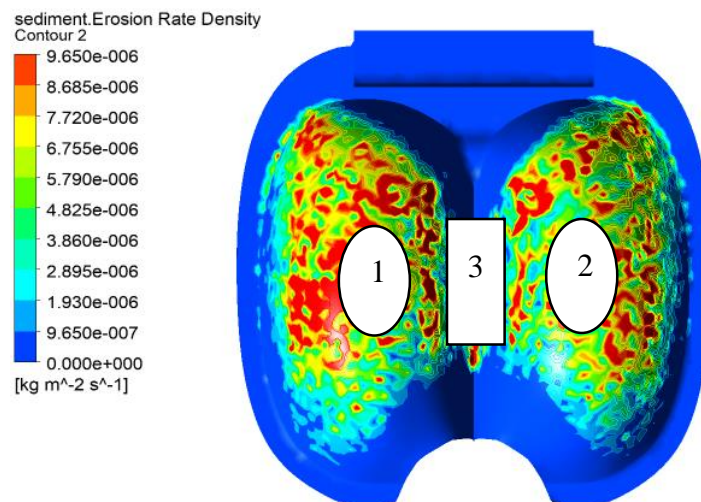

Figure 4.9: Accounted eroded area

4.3.2 Flow rate vs erosion

Tabakoff and Grant model has been used for predicting sediment erosion in the Pelton turbine buckets. In this thesis effect of flow rate on bucket erosion has been carried out at a different value of flow rate and keeping all other parameters constant. The variation of erosion is obtained from the CFX result is given in erosion rate density. The flow different pattern obtained from the simulation results are shown in following figure 4.10.These simulation revealed that the predicted erosion rate density increases with the increase in flow rate. This is due to the increase in flow turbulence and higher relative flow velocity at the bucket. To compare the simulation result with experiential result (Bajracharya T. , 2007) erosion rate density is converted into the mass loss by taking erosion-prone area and operating hours. The relation between erosion mass loss (in mg) and flow rate (in kg/s) is shown in figure 4.11. As shown in the graph it is found that as the value of flow rate increase mass loss also increased. For these particular value of flow rate the graph shown almost liner value.

(a) 2 kg/s   (b) 3 kg/s

(c) 5 kg/s   (d) 6 kg/s

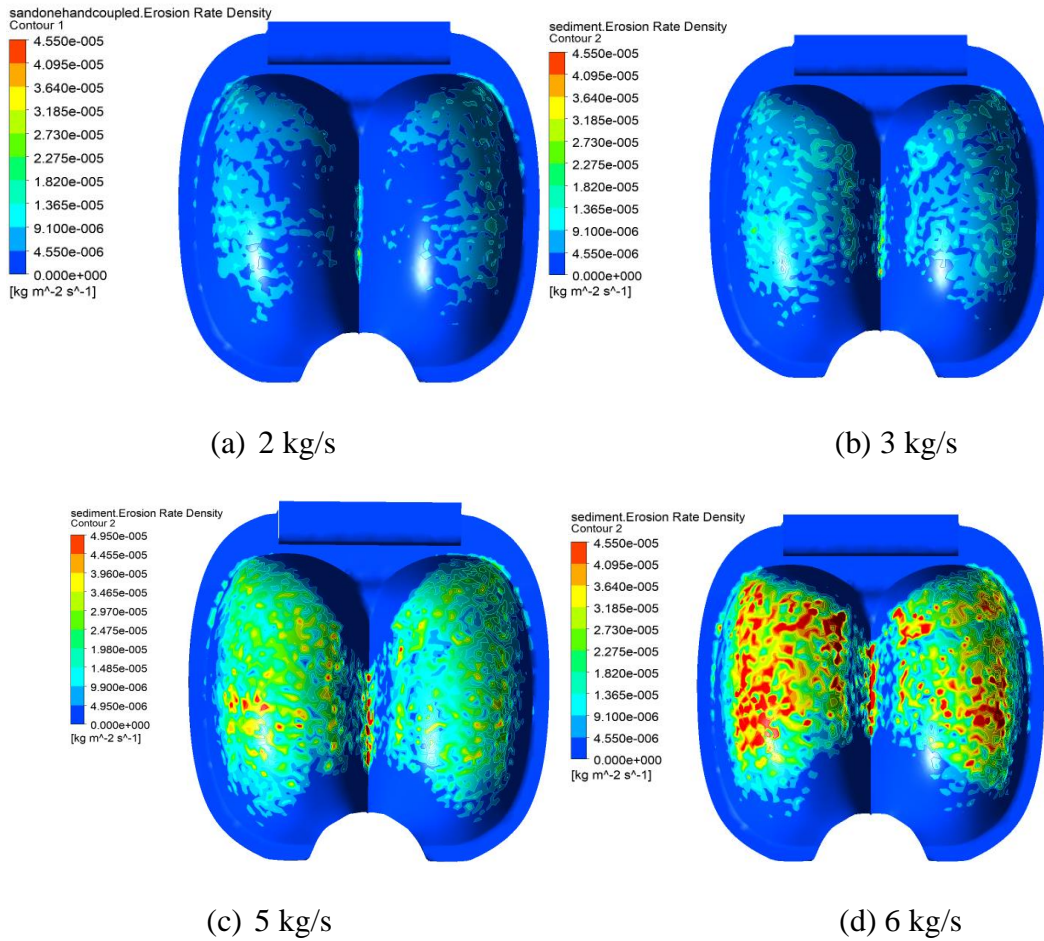Figure 4.10: Effect of flow variation on erosion rate density of Pelton turbine bucket

The value obtained from the numerical analysis is slightly greater than the experimental values. The main reason of the higher value of numerical result is that losses due to velocity profile at the jet nozzle is not considered in the numerical modelling.
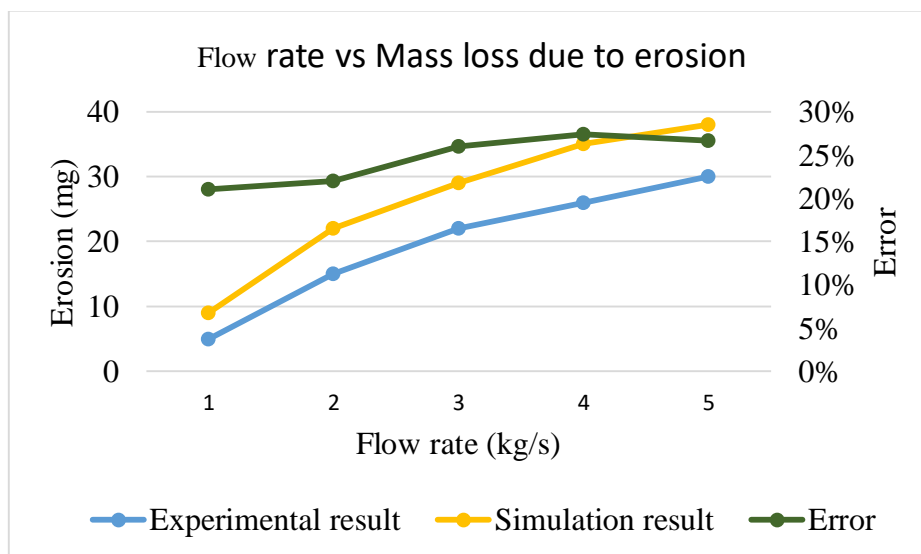

Figure 4.11: Mass loss in bucket due to flow variations

4.3.3 Particle concentrations vs Erosion

To find the effect of sediment particle concentration on Pelton turbine bucket erosion modelling is carryout at different particle concentrations at a constant flow rate 4 l/s. Based upon the simulation results obtained from Tabakoff erosion model, the effects of sediment concentrations on erosion rate density on a bucket are presented in Figure 4.12 (a-d). . The effect of erosion is found maximum at splitter and bucket depth. As a higher value of particle concentration. The erosion is shifted toward the outlet of the bucket. And intensity of erosion rate density also becomes high.

(a) 261 ppm (b) 428 ppm

(c) 1000 ppm (d) 1980 ppm

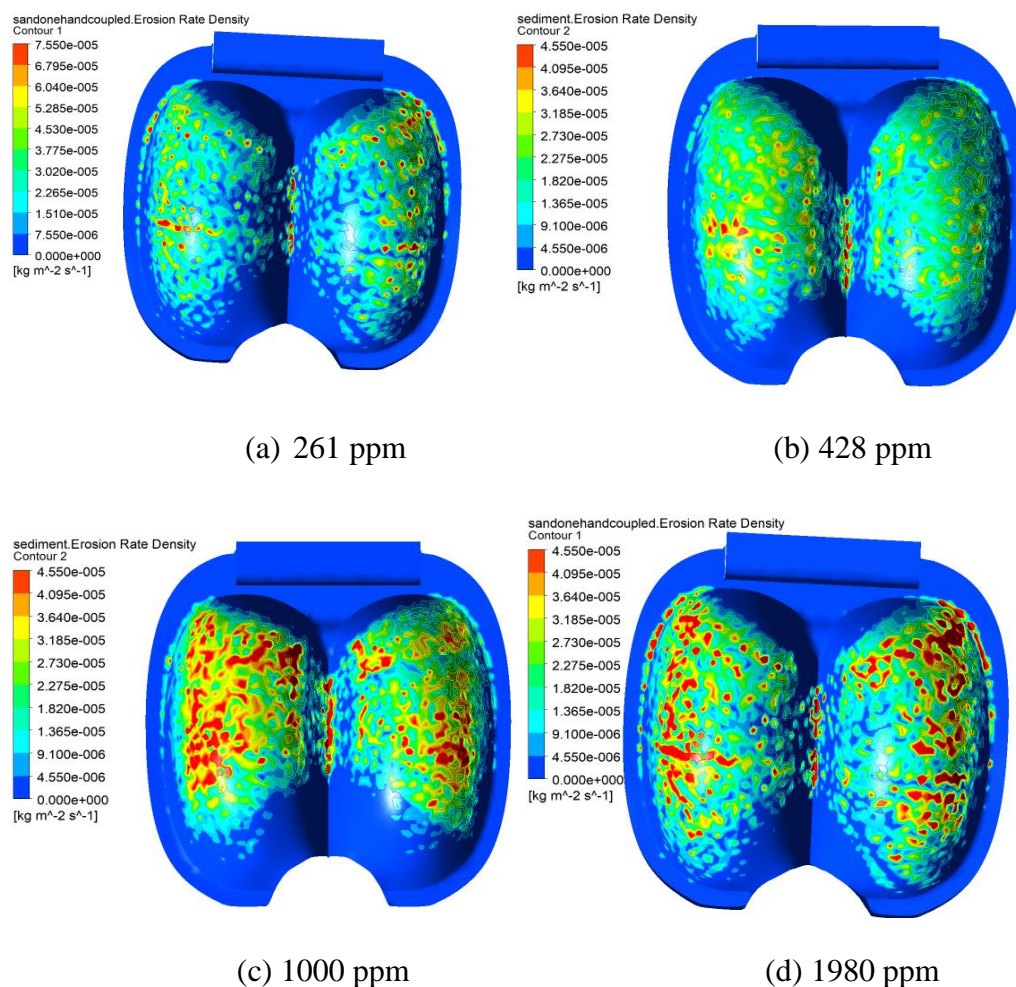Figure 4.12: Effect of particle concentration on erosion rate density of bucket

In order to investigate the effect of sediment concentration on erosion, different sediment concentration rate have been considered, while other parameters, i.e., sediment size, shape, operating condition of the turbine and impingement angle have been kept constant. It is observed from the figures that with the increase in particle

concentration rate, the erosion rate density increases. The variations of mass loss with particle concentration is presented in Figure 4.13. The erosion rate density obtained form numerical simulation is converted into mass mass loss by multiplying it with area and operating time. For these particular value it is seen that the mass loss due to erosion increases almost linearly with increasing the particle concentration rate. The result has been compared with experimental finding of (Bajracharya T. , 2007) and the the vlaue ontained form sumulation result is slightly deviated as compared with experimetal results. Error analyis has been carried out and the minimum error of 22% has been found at 261 pmm partciel concnetraion where as and maximum error has been occured at the 2000 ppm particle concentration.
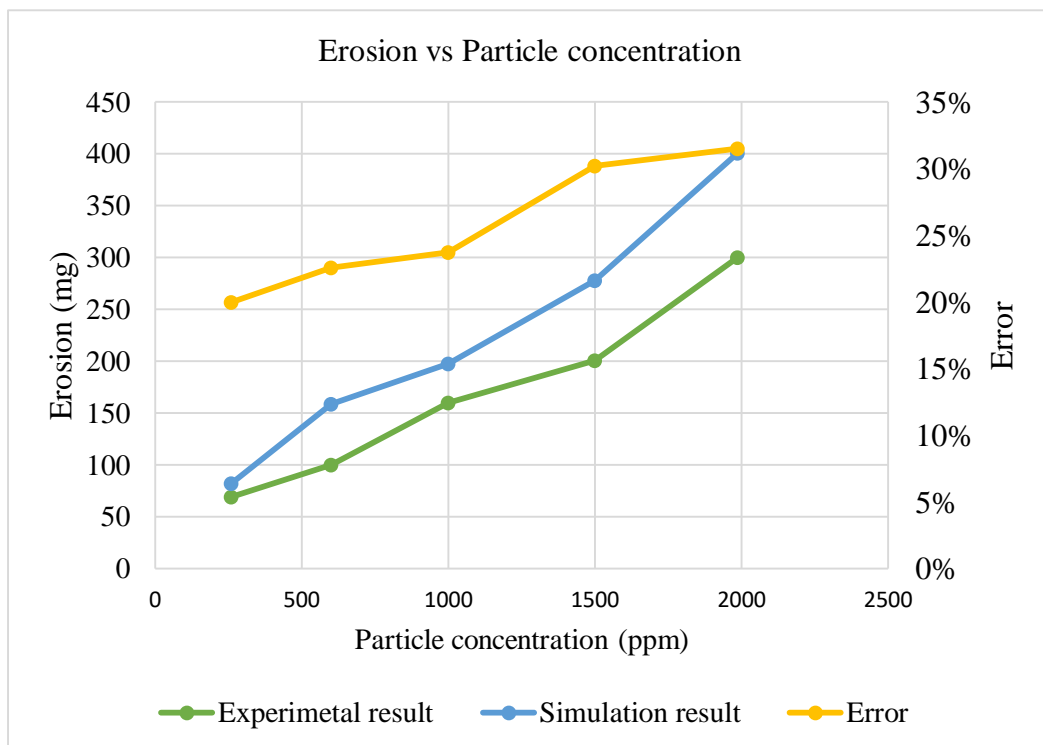
Figure 4.13: Effect of concentration rate on erosion of bucket

4.3.4 Efficiency deterioration

The torque generated by the runner is calculated by using the torque data produced by middle bucket. The torque distribution in middle bucket has been exported from ANSYS CFX, shown in Figure 4.14. Initially, torque is zero because water jet just starts to strike the bucket and later jet flow becomes steady and torque value reaches its peak point and then it reaches to steady-state condition which is found to be 10.99 Nm. As described in section 4.1.2, the efficiency of the Pelton turbine is calculated as 69%.
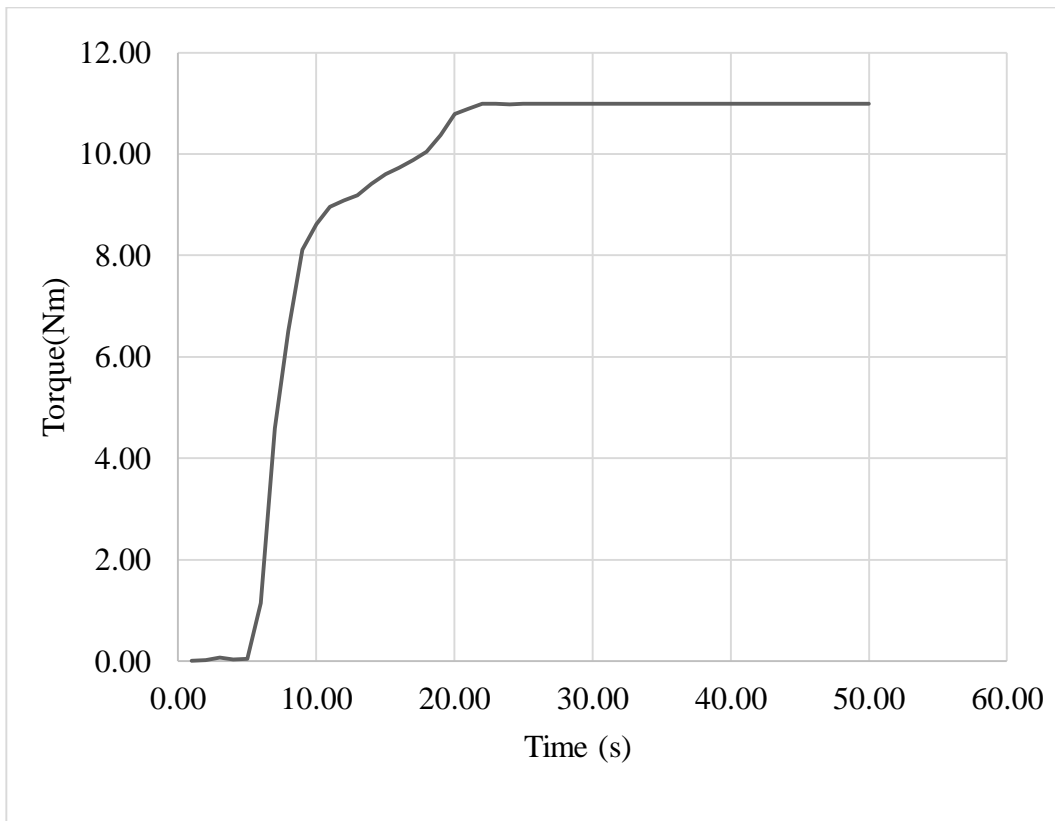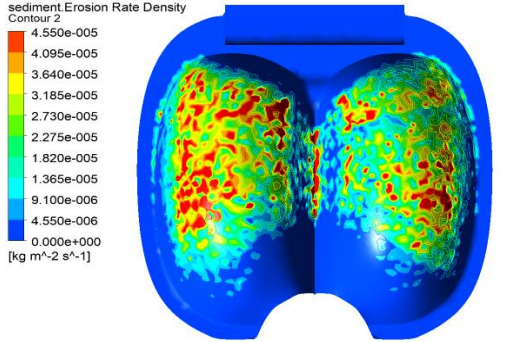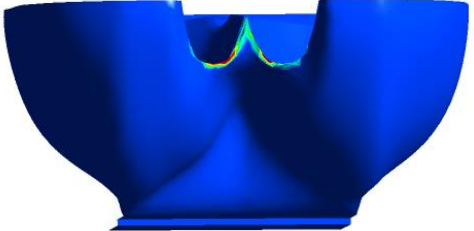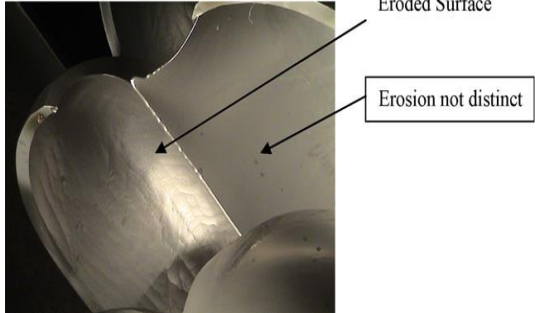
Figure 4.14: Steady state torque distribution in middle bucket

Table 4.2 shows the comparison of the erosion predicted from numerical modelling with the experimental and field study which was carried out by (Bajracharya T. , 2007) in his PhD. Thesis. The field study result carried out by him (Bajracharya T. , 2007) was from Khimti and Chilime Hydro power. From the findings, it can be concluded that the erosion model predicts the almost similar pattern with that of the experimental results. The maximum effect due to sediment was found in the area of splitter and depth of the bucket.

Table 4.2: Comparison of erosion predicated:

Numerical results	Experimental Results	Field study

CHAPTER FIVE: CONCLUSIONS AND RECOMMENDATIONS

5.1 Conclusions

The major findings of this thesis work are:

- The flow pattern in the Pelton turbine bucket has been numerically modeled for both transient and steady-state case and pressure contour and power have been calculated. The maximum pressure has been found to be $1.34*10^5$ Pa and the power has been found to be 1.81 kW which is 10% less than the maximum power (2 kW).

- The erosion pattern in the Pelton bucket has been analyzed using CFD modelling. It is the mass loss mainly occuring on the bucket depth and splitter. The backside of the bucket is also an erosion-prone area. The qualitative comparison of the erosion-prone area found from the numerical modelling has been observed to be similar with the literature and experimental result.

- The sand concentration and the flow rate have been found to be the major parameters for mass loss of the Pelton buckets, its variation has been found to be almost linear. From numerical analysis, mass loss in each bucket due to sediment particle has been found to be 82 mg for 4 l/s flow rate and 261 ppm particle concentration considering 72 operating hours and the deviation from the experimental value has been found to be below 20%.

- The efficiency of the turbine decreases with erosion due to the particle concentration. Experimentally, the efficiency of Pelton Turbine decreases by 1% due to the erosion. From the numerical modelling, it has been found that the efficiency of Pelton Turbine 69% considering erosion effect of erosion as compared to analytical and experimental value it is decreases by 6% and 4% in respectively. Which elucidates the error of 3% as compared to the experimental results. Sediment erosion analysis of Pelton turbine indicates relative erosion intensity and critical zones of erosion damage on the components of the turbine. The most realistic numerical prediction of the erosion has been found on the turbine bucket. The numerically obtained erosion pattern and experimental pattern of Pelton components are in good qualitative agreement. The agreement shows that, for this application, numerical simulation might be used really in a very predictive manner.

5.2 Recommendations

- For accurate results, it is recommended to use ICEM for meshing for numerical simulation.

- Velocity profile consideration by using user-defined function (UDF) for more accurate results is recommended.

- Transient simulation analysis is recommended for predicting the erosion on the turbine components, which was not possible during this study period due to the limitations in software and times.

- For power plant, it is recommended not to operate turbine during heavy flood season.

- It is recommended to carry out frequent routine maintenance and use of coating on bucket surface to reduce the effect of sediment erosion

REFERENCES

Dixon, S., & Hall, C. (2010). *Fluid Mechanics and Thermodynamics of Turbomachinery* (6th ed.). Oxford: Elsevier Inc.

Kleis , I., & Kulu, P. (2008). *Solid Particle Erosion Occurrence, Prediction and Control* (1st ed.). London: Springer-Verlag London Limited.

A.perrig, F. (2006). Flow in Pelton turbine Bucket:Numerical and Experimental Invetigation. *Trqansaction of ASME*, 128.

Amod Panthee, H. P. (2014). CFD Analysis of Pelton Runner. *IJSRP*, 2250-3153.

Anant Kr. Raia, A. K. (2017). Hydro-abrasive erosion in Pelton buckets: Classification and field study. *wear*, 8-20.

ANSYS Inc. (2017). *ANSYS CFX Theory Guide* (18.2 ed.). Southpointe: ANSYS Inc.

Bajracharya, T., Acharya, B., Joshi, C., Saini, R., & Dahlhaug, O. (2008). Sand Erosion of Pelton Turbine Nozzles and Buckets: A Case Study of Chilime Hydropower Plant. *Wear, 264*(3-4), 117-184.

Barstad, L. F. (2012). CFD Analysis of a Pelton Turbine(Master's Thesis). *NTNU*.

Biraj Singh Thapa a, B. T. (2012). Current research in hydraulic turbines for handling sediments. *Energy*, 62-69.

Chhetry , B., & Rana, K. (2015). Effect of Sand Erosion on Turbine Components: A Case Study of Kali Gandaki "A" Hydroelectric Project (144 MW), Nepal. *Hydro Nepal*, 24-33.

Chongji, Z., Yexiang, X., Wei, Z., Yangyang, Y., Lei, C., & Zhengwei, W. (2014). Pelton Turbine Needle Erosion Prediction Based on 3D Threephase Flow Simulation. *27th IAHR Symposium on Hydraulic Machinery and System* (pp. 1-7). IOP Conf. Series: Earth and Environmental Science.

D. AquaroE, F. (2001). Erosion of Ductile and Brittle Materials. *meccanica*, 651-661.

D., Aquaro, E. , & Fontani. (2001). Models of Erosion Analysis for Brittle and Ductile Materials. *Meccanica, 36*(6), 651-661.

Effect of size and concentration of silt particles on erosion of pelton turbine bucket . (n.d.).

Finnie, I. (1960). Erosion of Surfaces by Solid Particles. *Wear, 3*, 87-103.

Frawley, P., Corish, J., Niven, A., & Geron, M. (2009). Combination of CFD and DOE to Analyse Solid Particle Erosion in Elbows. *International Journal of Computational Fluid Dynamics, 23*(5), 411-426.

Hari Prasad Neopane, O. G. (2011). Sediment Erosion in Hydraulic Turbines. *GJRE*, 2249-4596.

IPPAN. (2018). *Hydropower in Nepal*. Retrieved July 13, 2018, from http://www.ippan.org.np/HPinNepal.html

J.U Brackbill, D. K. (1992). A continuum method for modeling surface. *Journal of Computational Physics,*, 335-354.

Javaheri, V., Portera, D., & Kuokkala, V.-T. (2018). Slurry erosion of steel – Review of tests, mechanisms and materials. *Wear, 408-409*, 248-273.

Jijian Lian, W. G. (2018). Effect of sediment size on damage caused by cavitation erosion and abrasive. *wear*, 201-208.

Laxman Poudel, B. T. (2012). Impact of Sand on Hydraulic Turbine Material: A Case Study of Roshi Khola, Nepal. *Hydro Nepal*.

leap australia . (2020, january). Retrieved from https://www.computationalfluiddynamics.com.au/turbulence-modelling/.

Lyczkowski, R. W., & Bouillard, J. X. (2002). State-of-the-art review of erosion modeling in fluid/solids systems . *Progress in Energy and Combustion Science, 28*(6), 543-602.

M.K. Padhy a, *. R. (2011). Study of silt erosion on performance of a Pelton turbine. *Energy*, 141-147.

M.K. Padhy, R. S. (2009). Effect of size and concentration of silt particles on erosion of pelton turbine bucket . *energy* , 1477–1483.

McLaury, B., & Wang. (1997). Solid Particle Erosion in Long Radius Elbows and Straight Pipes. San Antonio: SPE Annual Technical Conference and Exhibition.

Messa, G., Mandelli, S., & Malavasi, S. (2018). Hydro-abrasive erosion in Pelton turbine injectors: A numerical study. *Renewable Energy, 130*, 474-488.

Miners Foundry. (2016, march 17). Retrieved from https://minersfoundry.org/: https://minersfoundry.org/t/the-pelton-wheel/

NEA. (2019). *Annual Report.* Kathmandu: Nepal Electricity Authority.

Neopane, H. P. (2010). Sediment Erosion in Hydro,PhD. Thesis. *NTNU*.

Oka, Y., & Yoshida, T. (2005). Practical estimation of erosion damage caused by solid particle impact Part 2: Mechanical properties of materials directly associated with erosion damage. *Wear, 259*(1-6), 102-109.

Padhy, M. K., & Saini, R. (2008). A review on silt erosion in hydro turbines. *Renewable and Sustainable Energy Reviews, 12*(7), 1974-1987.

Pandit, H. P. (2005). Sediment handling at run-of-river projects in Himalayan rivers using sediment rating curves. *Nepalese Journal of Engineering, 1*(1), 39-45.

Pandya, D. (2013). Development of Computational Fluid Dynamics (CFD) Based Erosion Models for Oil and Gas Industry Applications. Arlington: The University of Texas at Arlington.

Panthee, A., Thapa, B., & Neopane, H. (2014). Quality Control in Welding Repair of Pelton Runner. *Renewable Energy, 79*(2015), 96-102.

Panthee, A., Thapa, B., & Neopane, H. P. (2014). CFD Analysis of pelton runner. *International Journal of Scientific and Research Publications (IJSRP), 4*(8), 50-55.

Poudel, L., Thapa, B., Thapa, B. S., Shrestha, B. P., Shrestha, K. P., & Shrestha, N. (2012). Computational and experimental study of effects of sediment shape on erosion of hydraulic turbines. Beijing: The 26thIAHR Symposium on HydraulicMachinery and Systems.

Rajput, R. (1999). *A Textbook of Hydraulic Machines: Fluid Power Engineering.* S. Chand.

Robin Thakur, S. K. (2019). Selection of Erosive Wear Rate Parameters of Pelton Turbine Buckets using PSI and TOPSIS Techniques. *IJITEE*, 2278-3075.

S., M. B. (2000). High-energy particle impact wear resistance of hard coating and their. *Wear*, 140-146.

Sailesh Chitrakar, H. P. (2018). A Review on Sediment Erosion Challenges in Hydraulic. *IntechOpen*.

Sailesh Chitrakar, H. P. (2019). River sedimentation challenges for hydropower development in Nepal: A. *SAARC* (pp. 5-6). Researchgate.

Saurabh Sangal, M. K. (2018). Hydro-abrasive erosion in hydro turbines: a review. *International journal of green energy*.

Srinivasan, V. (2014). Simulating Erosion Using ANSYS Computational Fluid Dynamics. ANSYS.

T.R. Bajracharya, B. A. (2008). Sand erosion of Pelton turbine nozzles and buckets:A case study of Chilime Hydropower Plant. *wear*, 264.

Tabakoff W., H. A. (1991). Effect of particle size distribution on. *ASME Jr. of Engg. for gas and*, 607-615.

Thapa, B. (2004). Sand erosion in hydraulic machinery, Phd Thesis. *NTNU*.

Thapar, O. (2002). Hydraulic Turbine Classification and Selection. In *Modern Hydroelectric Engineering Practice* (p. 53). 110: Alternate Hydro Energy Center.

White, F. (2006). *Viscous fluid flow. McGraw-Hill Higher Education.* New York NY: McGraw-Hill Higher Education.

Zhang, Z. (2016). Working Principle of Pelton Turbines. In *Pelton Turbine* (pp. 13-40). Springer.

APPENDIX A: Governing Equations

The governing equations of the CFD are Reynold's Averaged Navier Stoke Equation. The equations that are solved in the software during the simulation are following:

1. Conservation of mass (Continuity)

$$\frac{\partial \rho}{\partial t} + \rho \nabla V = 0)$$

<div align="right">Equation A1</div>

2. Conservation of momentum

$$\rho \frac{DV}{Dt} = \rho g + \nabla \tau_{ij} = \nabla p$$

<div align="right">Equation A2</div>

4. Conservation of energy

$$\rho \frac{Dh}{Dt} = \frac{Dp}{Dt} + \nabla(k \nabla T) + \phi$$

<div align="right">Equation A3</div>

Where, is the viscous stress tensor and Φ is the Dissipation function. $\frac{DV}{Dt} = \frac{\partial V}{\partial t} + (V.\nabla)V$ and tensor τ_{ij} for a Newtonian fluid is:

$$\tau_{ij} = \mu(\frac{\partial u_i}{\partial x_i} + \frac{\partial u_j}{\partial x_j})$$

<div align="right">Equation A4</div>

For incompressible fluid the continuity and momentum equation reduces to

$$\nabla . V = 0$$

<div align="right">Equation A5</div>

$$\rho \frac{DV}{Dt} = \rho g + \mu \nabla^2 V - \nabla p)$$

<div align="right">Equation A6</div>

5. RANS Turbulence Modeling

The fluid is assumed to be randomly unsteady turbulent state where any variable G is resolved to a mean value $\bar{G}$ plus a fluctuating value G'. The mean value is, by definition,

$$\bar{G} = \frac{1}{T}$$

<div align="right">Equation A7</div>

$$\overline{G} = \frac{1}{T} \int_t^{t+T} G dt$$

$$u = \bar{u} + u' \qquad v = \bar{v} + v' \qquad w = \bar{w} + w' \qquad p = \bar{p} + p' \qquad \text{Equation A8}$$

$$\bar{u} = \overline{(\bar{u} + u')} \qquad\qquad \text{Equation A9}$$

Where u, v, w and p are velocity components and pressure respectively.

Inserting above values, we obtain,

$$\frac{\rho D \bar{V}}{Dt} + \frac{\rho \partial}{\partial x_j} \left(u_i' u_j' \right) = \rho g + \nabla^2 \bar{V} - \nabla \bar{p} \qquad\qquad \text{Equation A10}$$

Rearranging this equation,

$$\frac{\rho D \bar{V}}{Dt} = \rho g + \nabla . \tau_{ij} - \nabla \bar{p}$$

Equation A11

Where,

$$\tau_{ij} = \mu \left(\frac{\partial u_i}{\partial x_j} + \frac{\partial u_j}{\partial x_i} \right) - \rho \, \overline{\left(u_i' u_j' \right)}$$
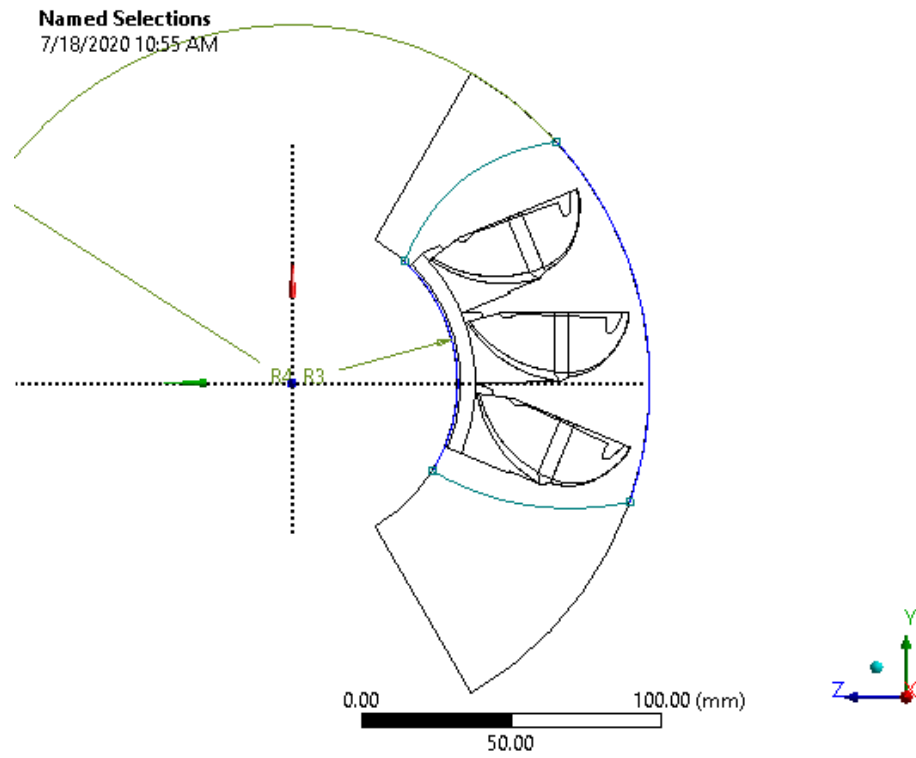
Figure B1: Sketch rotating Domain
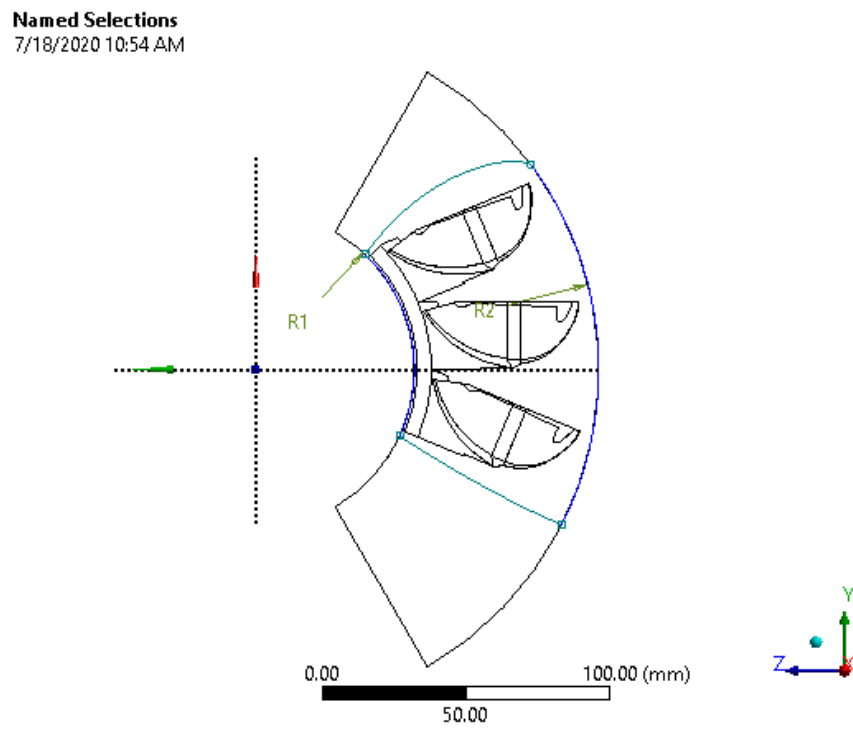
Figure B2: Sketch Body of Influence at splitter
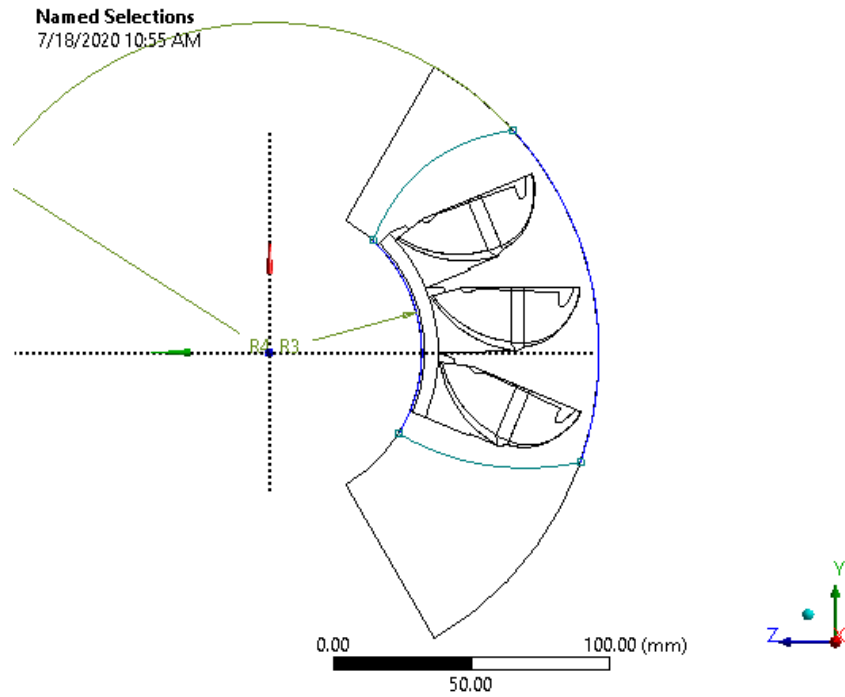
Figure B3: Sketch Body of Influence at outlet
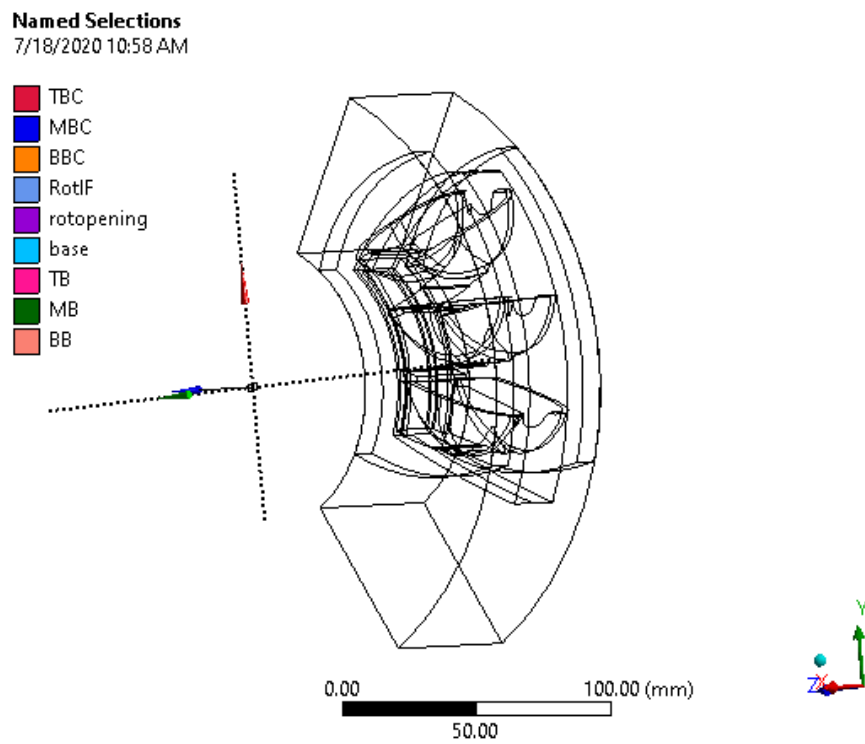
Figure B4: Rotating domain wireframe view

Figure B5: Rotating Domain
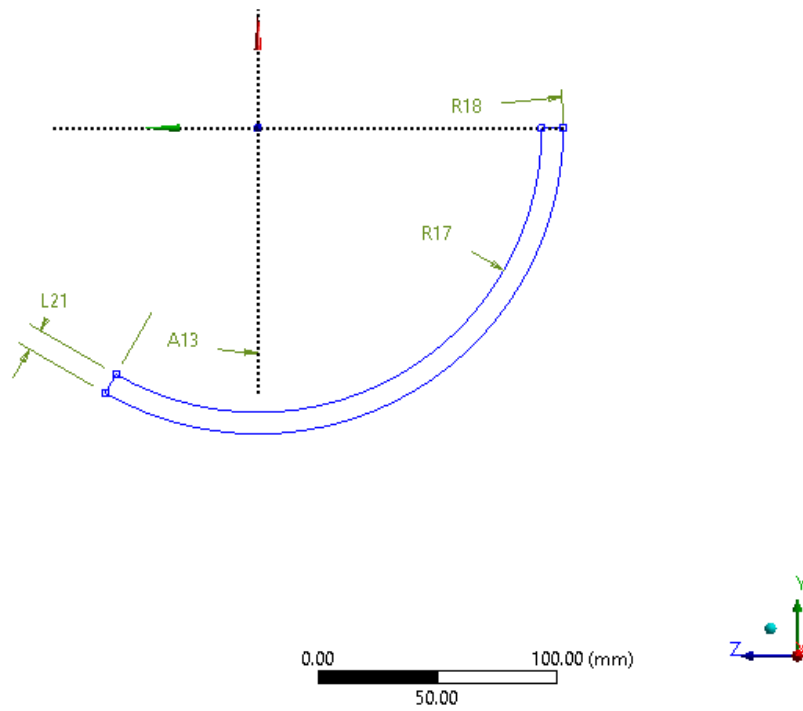
Figure B6: Sketch Stator

0.00   100.00 (mm)
50.00
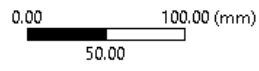
Figure B7: Sketch nozzle"

0.00   100.00 (mm)
50.00

Figure B8: Stationary Domain

APPENDIX C: Residual Results

Figure C1: Mass and momentum residuals

Figure C2: Turbulence residuals

Figure C3: Torque distibution

Figure C4: Erosion residual

70

APPENDIX D: Torque Data

Table D1: Time step torque data from simulation result

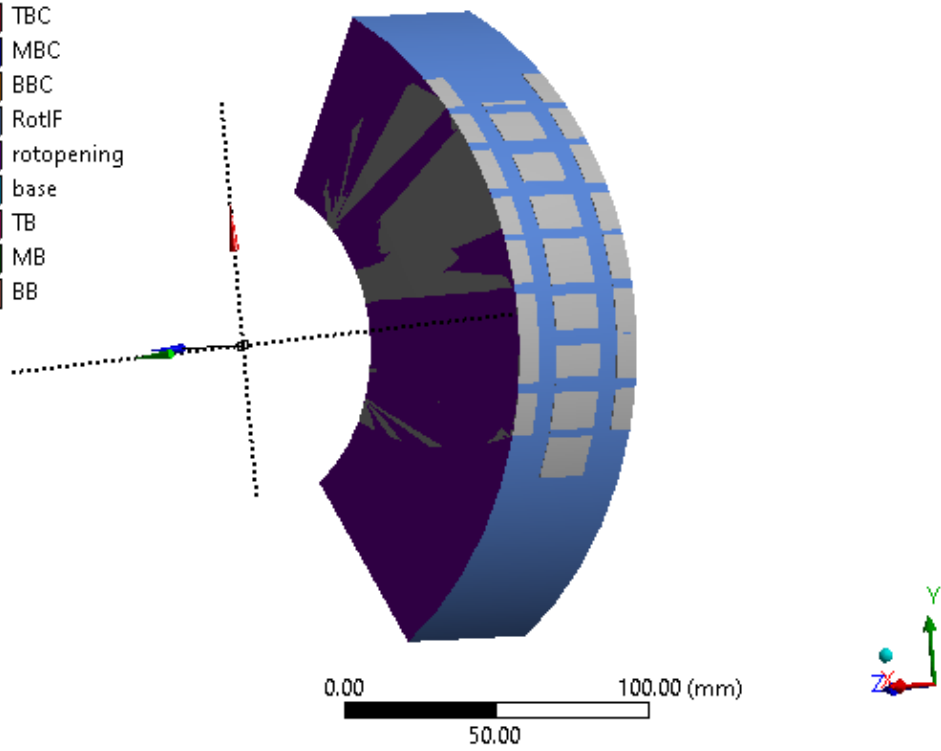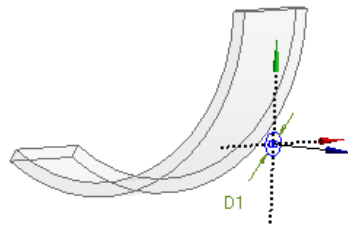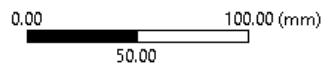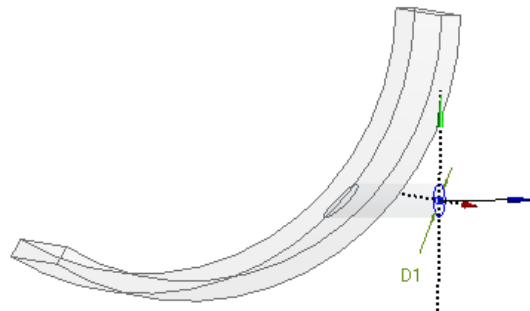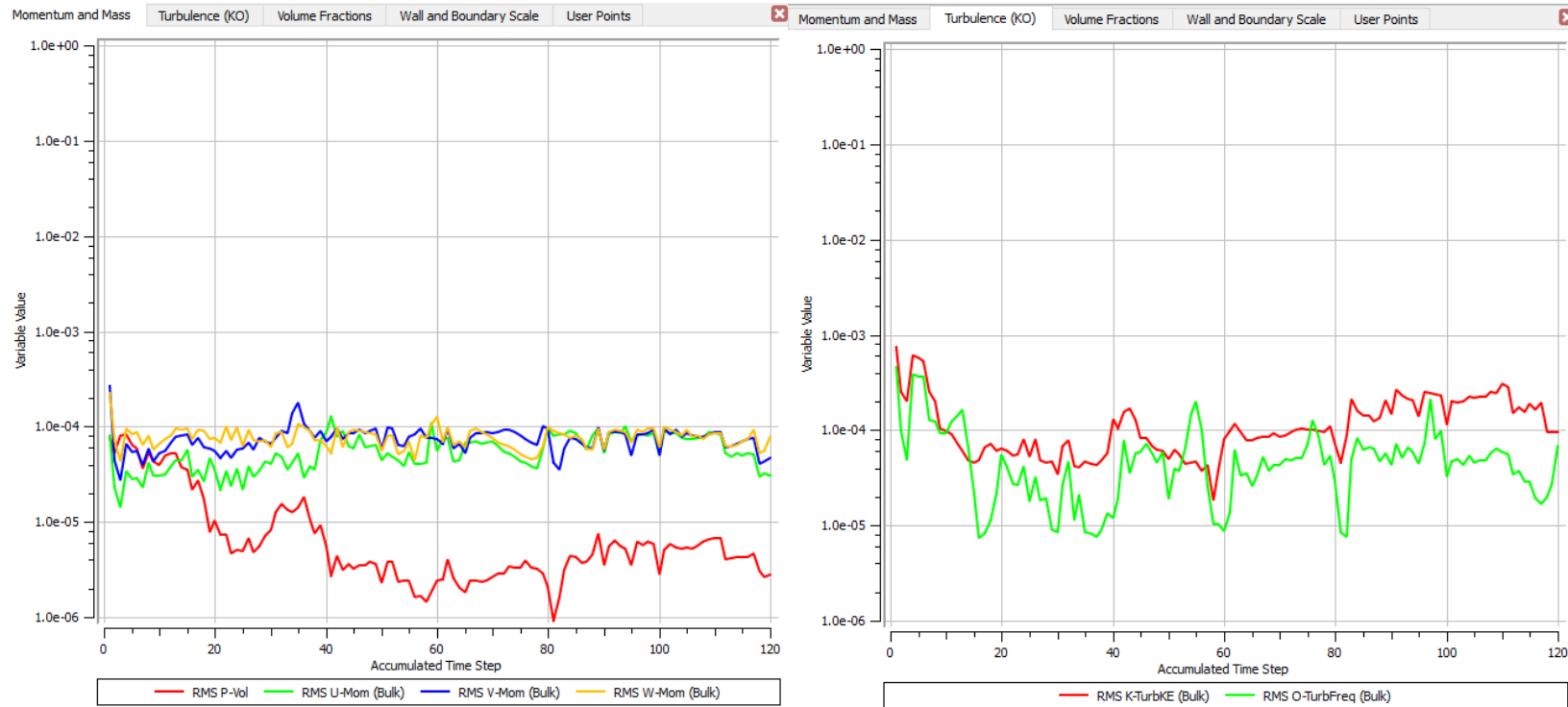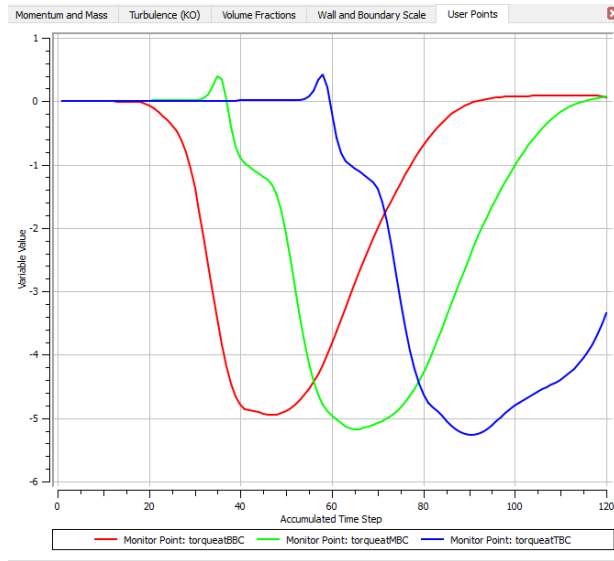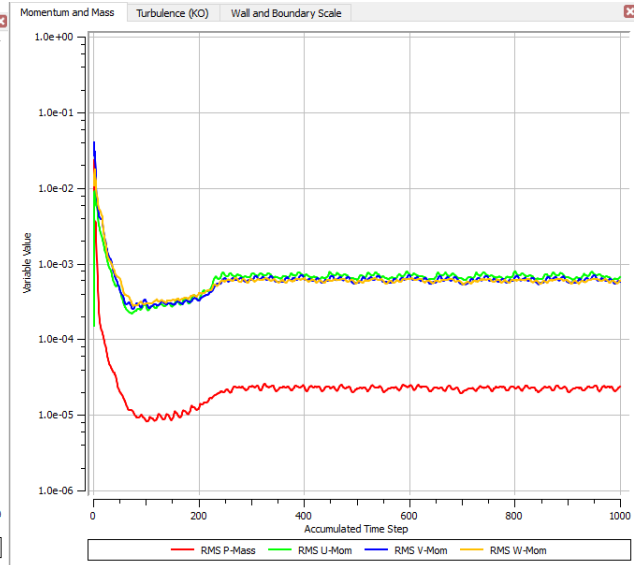| Time[s]	Torque(Nm)	time	torque	torque	torque	Time	torque
0.5	0.0181	22	0.0184	43.5	-1.44	65	-6.08
1	-0.00774	22.5	0.0189	44	-1.49	65.5	-6.07
1.5	0.000564	23	0.0193	44.5	-1.54	66	-6.06
2	0.0024	23.5	0.0197	45	-1.58	66.5	-6.04
2.5	0.00206	24	0.0202	45.5	-1.63	67	-6.03
3	0.00186	24.5	0.0207	46	-1.68	67.5	-6.01
3.5	0.00194	25	0.0212	46.5	-1.74	68	-6
4	0.00207	25.5	0.0215	47	-1.81	68.5	-5.98
4.5	0.00216	26	0.0222	47.5	-1.89	69	-5.97
5	0.00223	26.5	0.0228	48	-1.99	69.5	-5.95
5.5	0.00232	27	0.0235	48.5	-2.12	70	-5.94
6	0.00244	27.5	0.0244	49	-2.27	70.5	-5.92
6.5	0.00256	28	0.0254	49.5	-2.45	71	-5.91
7	0.0027	28.5	0.0271	50	-2.66	71.5	-5.89
7.5	0.00286	29	0.03	50.5	-2.88	72	-5.87
8	0.00304	29.5	0.0343	51	-3.12	72.5	-5.85
8.5	0.00324	30	0.0406	51.5	-3.37	73	-5.83
9	0.00347	30.5	0.0493	52	-3.63	73.5	-5.8
9.5	0.00372	31	0.0601	52.5	-3.88	74	-5.77
10	0.004	31.5	0.0726	53	-4.12	74.5	-5.73
10.5	0.00432	32	0.0857	53.5	-4.35	75	-5.68
11	0.00479	32.5	0.103	54	-4.57	75.5	-5.63
11.5	0.00549	33	0.132	54.5	-4.77	76	-5.56
12	0.00629	33.5	0.176	55	-4.96	76.5	-5.49
12.5	0.00704	34	0.231	55.5	-5.14	77	-5.41
13	0.00775	34.5	0.285	56	-5.3	77.5	-5.33
13.5	0.00847	35	0.305	56.5	-5.44	78	-5.23
14	0.00931	35.5	0.267	57	-5.56	78.5	-5.14
14.5	0.0101	36	0.168	57.5	-5.66	79	-5.04
15	0.0109	36.5	0.032	58	-5.73	79.5	-4.93
15.5	0.0116	37	-0.127	58.5	-5.79	80	-4.82
16	0.0125	37.5	-0.293	59	-5.85	80.5	-4.72
16.5	0.0133	38	-0.452	59.5	-5.91	81	-4.61
17	0.014	38.5	-0.593	60	-5.95	81.5	-4.5
17.5	0.0149	39	-0.715	60.5	-5.99	82	-4.39
18	0.0157	39.5	-0.819	61	-6.03	82.5	-4.28
18.5	0.0163	40	-0.916	61.5	-6.05	83	-4.17
19	0.0169	40.5	-1.01	62	-6.07	83.5	-4.07
19.5	0.0173	41	-1.11	62.5	-6.08	84	-3.96

20	0.0174	41.5	-1.19	63	-6.09	84.5	-3.86
20.5	0.0175	42	-1.26	63.5	-6.09	85	-3.76
21	0.0177	42.5	-1.32	64	-6.09	85.5	-3.66
21.5	0.018	43	-1.38	64.5	-6.09	86	-3.56
86.5	-3.46	108.5	-0.318				
87	-3.36	109	-0.287				
87.5	-3.26	109.5	-0.257				
88	-3.17	110	-0.229				
88.5	-3.07	110.5	-0.202				
89	-2.97	111	-0.176				
89.5	-2.87	111.5	-0.151				
90	-2.77	112	-0.128				
90.5	-2.67	112.5	-0.106				
91	-2.57	113	-0.086				
91.5	-2.48	113.5	-0.0669				
92	-2.38	114	-0.0489				
92.5	-2.29	114.5	-0.0317				
93	-2.2	115	-0.0155				
93.5	-2.11	115.5	0.000184				
94	-2.02	116	0.0158				
94.5	-1.93	116.5	0.0311				
95	-1.85	117	0.0466				
95.5	-1.77	117.5	0.0624				
96	-1.69	118	0.0773				
96.5	-1.61	118.5	0.0916				
97	-1.54	119	0.105				
97.5	-1.47	119.5	0.116				
98	-1.4	120	0.127				

```
source = Torque data;
target = 0.001;
nt = 10;
g = 9.81;
R = 87.5;
Z = 16;
H = 40;
c1 = 0.981*sqrt(2*g*H);
angularvelocity = (c1/(R))*1000;
f = (angularvelocity*Z)/(2*pi);
dt = 1/f; %Bucket period [s]
T_temp(1,1) = 0;
T_temp(2:size(source,1)+1,1) = source(:,3);
T_temp(1,2) = 0;
T_temp(2:size(source,1)+1,2) = source(:,2);
clear source
for i = 2:size(T_temp(:,1),1)
T_temp(i,3) = T_temp(i,1)-T_temp(i-1,1);
end
min_step = min(T_temp(2:end,3));
%Total time
t_tot = T_temp(end,1);
error = 1;
timestep = 1;
i = size(T_temp(:,1),1);
while error>= target
timestep = t_tot/i;
shift = round(dt/timestep);
%Error
error = abs((dt-timestep*shift)/timestep);
%error = abs((dt?timestep*shift)/dt);
if timestep > 0.5*min_step
error = 1;
end
  if error >=target
i = i + 1;
else
    break
  end
end
%Create timeline in torque matrix T
T(:,1) = 0:timestep:(t_tot+(nt*dt));
%Create spline of the original torque source
Ts(:,1) = 0:timestep:T_temp(end,1);
Ts(:,2) = spline(T_temp(:,1),T_temp(:,2),Ts(:,1));
%Insert the torque series in T matrix
L = size(Ts,1);
for k = 1:nt
if k == 1
T(1:L,k+1) = Ts(:,2);
else
T(shift*(k-1):shift*(k-1)+L-1,k+1) = Ts(:,2);
end
end
```

```
p = find (T(:,k+1)~=0);
p = p(end);
for g = 1:p
T(g,k+2) = sum(T(g,2:k+1));
end
T(p+1:size(T,1),:) = [];
clear Ts k nt p L g T_temp
%?????? END ??????
```

APPENDIX F: Originality Report

Anil_IV

ORIGINALITY REPORT

16%	10%	8%	12%
SIMILARITY INDEX	INTERNET SOURCES	PUBLICATIONS	STUDENT PAPERS

PRIMARY SOURCES

1	brage.bibsys.no Internet Source	2%
2	Submitted to Seoul National University Student Paper	2%
3	docplayer.net Internet Source	1%
4	Submitted to Institute of Engineering, Pulchock Campus, Tribhuvan University Student Paper	1%
5	www.tandfonline.com Internet Source	1%
6	T.R. Bajracharya, B. Acharya, C.B. Joshi, R.P. Saini, O.G. Dahlhaug. "Sand erosion of Pelton turbine nozzles and buckets: A case study of Chilime Hydropower Plant", Wear, 2008 Publication	1%
7	Submitted to Curtin University of Technology Student Paper	<1%

mafiadoc.com

| 8 | Internet Source | <1% |

| 9 | Felix A. Ishola, Joseph Azeta, George Agbi, Obafemi O. Olatunji, Festus Oyawale. "Simulation for Material Selection for a Pico Pelton Turbine's Wheel and Buckets", Procedia Manufacturing, 2019
Publication | <1% |

| 10 | www.diva-portal.org
Internet Source | <1% |

| 11 | Submitted to Universiti Tenaga Nasional
Student Paper | <1% |

| 12 | Submitted to Universiti Malaysia Kelantan
Student Paper | <1% |

| 13 | M.K. Padhy, R.P. Saini. "Study of silt erosion mechanism in Pelton turbine buckets", Energy, 2012
Publication | <1% |

| 14 | Z Chongji, X Yexiang, Z Wei, Y Yangyang, C Lei, W Zhengwei. "Pelton turbine Needle erosion prediction based on 3D three- phase flow simulation", IOP Conference Series: Earth and Environmental Science, 2014
Publication | <1% |

| 15 | Sailesh Chitrakar, Bjørn Winther Solemslie, Hari Prasad Neopane, Ole Gunnar Dahlhaug. | |

APPENDIX G: Paper Published

Paper published in journal as a part of the work with in thesis is presented in the following section

NUMERICAL STUDY ON SEDIMENT EROSION 0F MICRO PELTON TURBINE BUCKETS

T.R. Bajracharya*[1], A.K. Pachhain*[2], A. Sapkota*[3], A.B. Timilsina*[4]

*[1]Professor, Department of Mechanical Engineering, Pulchowk Campus, Institute of Engineering Tribhuvan University, Nepal

[2][3] Department of Mechanical Engineering, Pulchowk Campus, Institute of Engineering Tribhuvan University, Nepal

*[4] Center for Energy Studies, Institute of Engineering, Tribhuvan University, Nepal

ABSTRACT

Most of the hydropower plants built in the Himalayan originating rivers contain an enormous amount of sediment in them with the domination of hard minerals. These hard minerals in the sediment is the major reason for hydro-abrasive erosion of hydro-mechanical and turbine components. The nature and severity of the erosion depends upon the nature and physical properties of the sediment and the operating environment as well. Pelton turbine plays a convincing role in high head hydropower plants. In case of a Pelton turbine, the injector, splitter and bucket surface-front and back are typical erosion areas. The direct effect of erosion is loss of efficiency and mechanical vibration eventually leading to failure. In this study, using a commercial CFD code, erosion in a micro Pelton turbine (2 kW) is analyzed by first simulating the transient state and then the steady-state flow behavior of the Pelton turbine. The flow modeling was done with SST turbulence model with interphase transfer method as a free surface and mixture model and erosion modeling was done with Tabakoff and Grand erosion. As seen on the experimental studies, the erosion rate density was found to be maximum at the bucket splitter and noticeable erosion was seen in the bucket front and backside. For comparison purpose, mass loss was evaluated from the computed erosion rate density and was compared with the experimental one.

KEYWORDS: Pelton Turbine, CFD, Erosion, SST Model, Turbulent Model, Efficiency

I.   INTRODUCTION

Pelton turbine is a high head impulse type turbine. Being an impulse type turbine, the energy harness in the turbine takes place in two stages, first the conversion of the potential energy of the water into kinetic energy and secondly the high speed jet striking the runner imparting its kinetic energy to the rotational kinetic energy of the runner. Nozzle-Needle, Runner and the Casing are the major parts of a Pelton turbine. These parts are the parts of water flow channel hence are exposed to the sediment laden water. One can thus expect to see hydro-abrasive erosion in these areas. In Himalayan originating rivers in South-Asia, the influence of heavy rains during the monsoon period (June–September) causes wide variation in river flows and the rainfall is also the cause for land erosion, and landslides thus producing high sediment content in the rivers. The presence of hard minerals in the river sediment can be owed to the fragmentation of rock due to chemical and mechanical weathering which during monsoon period is carried by the river. The sediment content in the river is seasonal and is maximal during the monsoon season and minimal during the dry season [1, 5].

Thus during the monsoon season, enormous amount of these sediment particles reach the turbine parts and cause erosion. In case of a Pelton turbine, the injector, bucket splitter, front and back side of bucket suffer erosion. The direct effect of this erosion is loss of efficiency hence is an economically important issue as there is generation loss. A field setting research revealed the erosion rate of 3.4 mm/year for the needle and the bucket resulting in an efficiency reduction of 1.21% and as a consequence loss in the power generation for Chilime Hydropower Plant in Nepal [2].

The erosion caused by the suspended sediment in water falls under the category of solid particle erosion. The suspended particles gain the velocity of the host fluid and impact on the solid surface causing the removal of small fragments of the solid. In case of the sediment laden water, the silt particles are designated responsible for erosion. These particles remove the base material of the runner, altering the runner profile (loss of hydraulic efficiency)

and also weakens the runner structure. Literature classify the nature of erosion seen in the Pelton turbine bucket as

• Plastic deformation and indentation, overlapping craters at the splitter tip

• Plastic deformation as well as by ploughing

Thapa and Brekke, 2004, concluded that fine particles such as silts cause erosion on the needle but not much erosion in the buckets and if the particles are coarse (sand) then there will be more erosion in the buckets and less erosion of needle. Sand with medium size particles will cause erosion of both needle and bucket [3, 4]. The percentage efficiency loss of a Pelton turbine increases with an increase in the silt concentration, silt size, and jet velocity. The direct effect of erosion is loss of the bucket mass, this loss results in a decrease of the turbine mechanical power output [5, 6]. Due to the erosion the generation loss, repair, maintenance loss imposes a heavy loss of capital along with the danger of premature failure of turbine components compared to their estimated life expectancy thus to have reliable investments for hydropower development in a country, the challenges of sediment erosion in hydro mechanical components especially of turbines need to be addressed with a sustainable solution. Computational Fluid Dynamics (CFD), is a branch of fluid dynamics that uses numerical methods and algorithms to solve fluid flow problems [8]. Reduction of time and cost to predict the model behavior in a real environment is the key advantage of CFD analysis so it can be best the option to minimize the dependency in the experimental analysis which is highly time-consuming and costly. Many researchers have applied CFD as a numerical analysis tool for analyzing flow behaviour in the Pelton turbine component mainly buckets and injector.

In this study, erosion in a 2 kW Pelton turbine bucket is analyzed using commercial CFD code ANSYS CFX and is compared against the experimental findings. For flow validation, the torque applied to a non-stationary Pelton bucket, subject to a high-speed water jet is predicted and compared against the experimental one. Numerical modeling of the three buckets are used and Tabakoff and Grant erosion model is applied to model the quantitative and qualitative nature of the erosion.

II. METHODOLOGY

The methodology used for this study is shown in Figure 1. The method adopted for any CFD simulation process contains three stages (i) pre-processing, (ii) solution and (iii) post-processing. The 3D model of the Pelton turbine
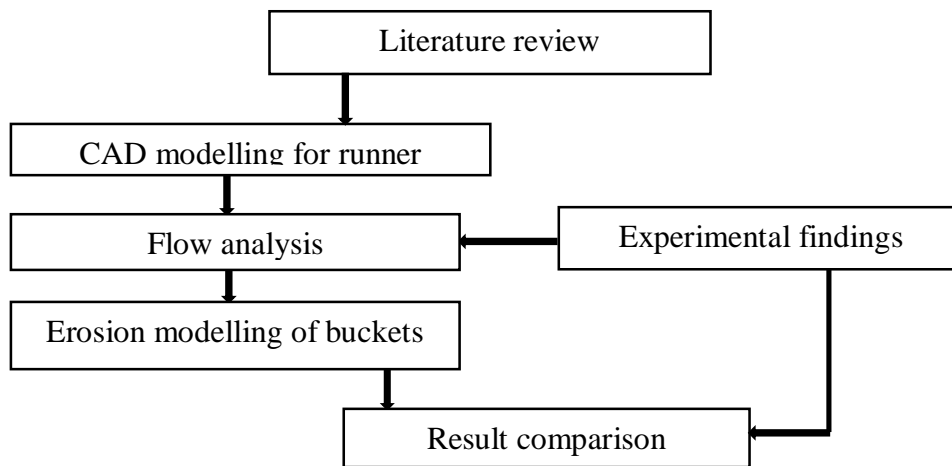
Figure: 1 Methodology for CFD analysis

was created with reference to a model turbine at a laboratory test facility. The 3-D model of the bucket is created in CATIA V5R20. Then the fluid model consists of a rotating domain and the stationary domain for CFD analysis was modeled using ANSYS Design Modeler. The numerical methods and boundary conditions were defined in ANSYS CFX on the basis of the experimental procedure. Numerical results were validated by comparing with the experimental findings.

III.   NUMEERICAL ANALYSIS

CAD model of bucket was developed from the CATIA V5R20. Bucket profile is based in the scaled Pelton turbine available in IOE Pulchowk campus. And In the numerical methods boundary conditions and all setup are taken with reference with the experimental.

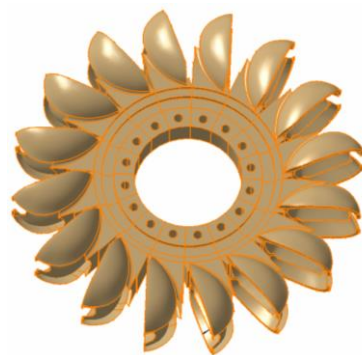**Table 1.** Specification of turbine

| Type	Pelton Turbine
Make	Balaju Yantra shala
No. of Bucket	16
Runner PCD	175mm
Maximum power output	2kw

a)   Bucket 3-D model and Fluid domain

Pelton Bucket is scanned from 3-D scanner Einscan pro 2x. It does offer an impeccable scanning accuracy of up to 0.02mm. A Scanned file is then imported in CATIA V5 and the CAD model is created with reference to this original scanned bucket as in figures 2 and 3. The physical setup shown in figures 4 and 5 is a sketch based on a method DynaVec has experimented with [11]. The main concept of this method is that the middle bucket is subject to one, complete water-jet cycle, and data obtained from this bucket can be used to model for the total runner. The domain is defined by the rotating domain, stationary domain with a nozzle. The Modeled domain was created in ANSYS 18.1 own CAD modeling application, DesignModeler. Three Pelton buckets geometry was placed inside the rotating domain, and the volume this geometry occupies is subtracted from the rotating domain by using Boolean application. The dimension of both rotating and stationary domain is set at 120 degree which quarter of a disk with three hollows. The geometric simplifications of this method is the lack of a turbine casing and the injector components. In this paper, the three-bucket approach is used because the computational cost is a limiting factor and simplicity for the study.
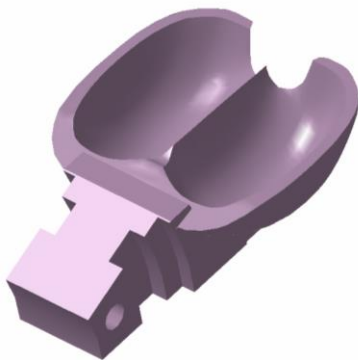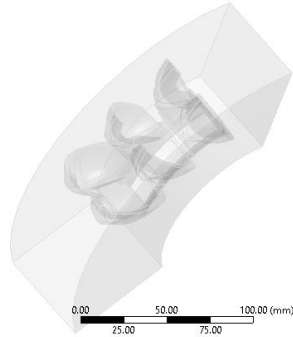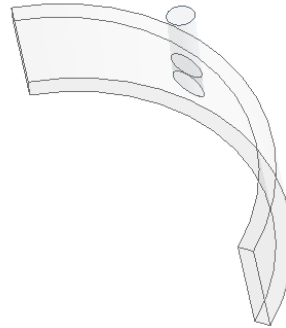
Figure: 2 3-D model of bucket and turbine   **Figure: 3** Selected bucket for analysis
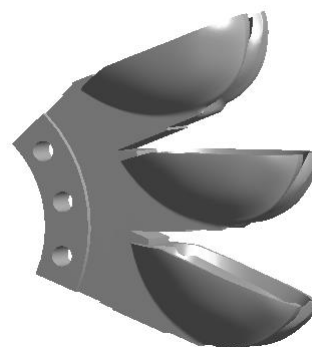
Figure: 4 Rotating fluid domain   **Figure: 5** Stationary domain

b)   Meshing

The meshing of the physical domain was carried out in ANSYS 18.1 meshing. Fluid domain was divided into two separate components, one for the stationary domain and one for the rotating domain. The main reason to divide two standalone components was rotating domain was meshed with an advanced size function, while the stationary domain did not use this function. The stationary is done fine mesh around the jet region with prismatic element of element size of 1 mm and the whole domain consists mostly of hexahedral elements of maximum size of 3mm. An inflation in the radial direction of jet wall region. The rotating domain was meshed with the advanced size function "Proximity and Curvature" and consists mainly of tetrahedral elements body of influence is used at water jet inlet and water outlet with fine mesh. The "body of influence" of size 1mm is used as shown in figure 6 to increase the element density in this area.
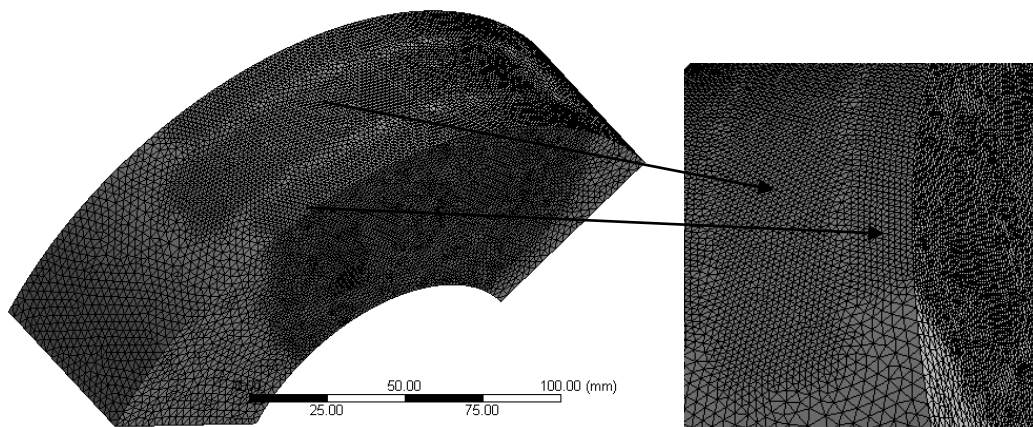
Figure: 6 Meshed rotating domain with body of influence
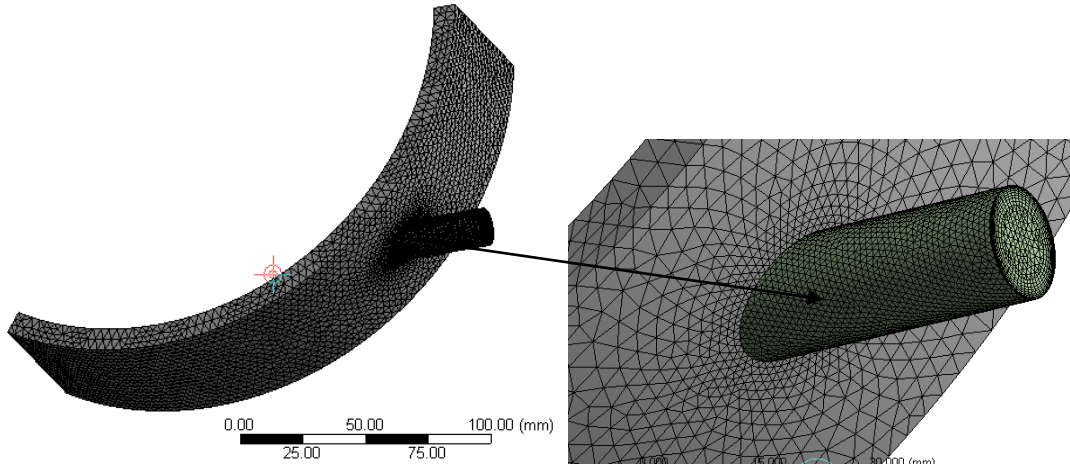
Figure: 7 Meshed stationary domain

c) Erosion model for simulation

In the erosion model of Tabakoff and Grant, the erosion rate E is determined from the following relation [8].

$$E = k_1 f(\gamma) V_P^2 \cos^2 \gamma \ [1 - R_t^2] + f(V_{PN}) \tag{1}$$

Where;

$$f(\gamma) = \left[1 + k_2 k_{12} \sin\left(\gamma \frac{\pi/2}{\gamma_0}\right)\right]^2 \tag{2}$$

$$R_T = 1 - k_4 V_P \sin\gamma \tag{3}$$

$$f(V_{PN}) = k_3 (V_P \sin \gamma)^4 \tag{4}$$

$$k_2 = \begin{cases} 1.0 & if\ t \leq 2\gamma_0 \\ 0.0 & if\ \gamma > 2\gamma_0 \end{cases} \tag{5}$$

Here, E is the dimensionless mass (mass of eroded wall material divided by the mass of particle) V_P is the particle impact velocity γ is the impact angle in radians between the approaching particle track and the wall, γ_0 being the angle of maximum erosion. k_1, to k_4, k_{12} and γ_0 are model constants and depend on the particle/wall material combination. To make the model more general, the model is rewritten so that all model constants have a dimension of velocity. The following list shows the link between the constants of the original model and those in CFX

Table 2. Constants in Tabakoff and Grant erosion model.

Value	Dimensions	CFX-Pre Variable
K_{12}	(dimensionless)	K12 Constant
K_2	(dimensionless)	
V_1	[Velocity]	Reference Velocity 1
V_2	[velocity]	Reference Velocity 2
V_3	[Velocity]	Reference Velocity 3

γ_0	[degree]	Angle of Maximum Erosion

Where,

$$V_1 = 1/\sqrt{k_1} \tag{7}$$

$$V_2 = 1/ (\sqrt[4]{k_3}) \tag{8}$$

$$V_3 = 1/k_4 \tag{9}$$

The erosion of a wall due to a particle is computed from the following relation:

$$Erosion\ Rate = E * N * m_P \tag{10}$$

Here m_p is the mass of the particle and N is its number rate. The overall erosion of the wall is then the sum over all particles. This gives an erosion rate in kg/s, and an erosion rate density variable in the res file and post-processor in $kg/s/m^2$ .Note that this erosion rate is only a qualitative guide to erosion, unless precise values for the model constants are known.

d) Numerical Setup

Steady-state analysis type is selected as less computational time needed. Only two phase mixture of water and sediment particle is considered. Shear Stress Transport (SST) model is also the two-equation model blending the free stream advantages of the k-ω model with the wall bounded advantages of the k-ε model. SST turbulence model with automatic wall function was used as good convergence was required in both near the wall region and region far away from the wall [7-9]. Pressure in Pelton turbine is always around atmospheric so reference pressure in both domains were set 1 atm. Two fluid domains were created, one for the rotating part and one for the stationary part. And relative pressure between inlet and outlet was set 0 atm. Therefore particles were modeled based on sand analysis which was carried in an experimental study in 2008. The density of quartz is 2650 kg/m^3 and Molar mass of 1 kg/kmol is used. The diameter of the particle has the minimum for 0.05 mm, maximum for 0.15 mm with an average value of 0.1 mm. Tabakoff and Grand erosion model was used and fully coupled particle coupling of sediment particle and water is selected [8].

The interface model General Connection and the frame change/mixing model Frozen Rotor Stator were chosen and the pitch ratio was set manually to 1.To apply a rotation to the rotating domain, Domain Motion in the rotating domain was set to Rotating, with the value of 1430 rpm in the clockwise direction of the x-axis is used. All three buckets were defined as no slip, smooth walls. Mass flow rate inlet is defined for the jet with a value of 4 kg/s and particles mass flow rate of 0.001004 kg/s with reference from the experimental data. No slip, smooth wall near jet region which gives better jet stability [6]. Opening boundary of relative pressure 0 atm. was defined in other part of the domain.

IV.　　RESULTS AND DISCUSSION

a) Prediction of Erosion

The pressure distribution due to water jet in the middle bucket is shown in Figure 8(a). It was found that the maximum pressure of $1.317*10^5$ Pa is obtained at the splitter and PCD of the bucket. The pressure peak obtained in bucket splitter is due to the initial impart of the jet. It is obvious to obtain the maximum pressure at bucket PCD since the Pelton runner is designed such that it would convert most of the hydraulic energy to mechanical energy when the jet strikes at the PCD of the bucket of the runner [12]. Figure 8 (b) shows the particle tracks and the streamlines from the jet inlet. The black lines are particle tracks and other lines are streamlines of water. They are roughly the same, distribute uniformly and continuously. This may mainly result from a uniform inlet and small particle diameter which leads to smaller inertial force than interaction force.
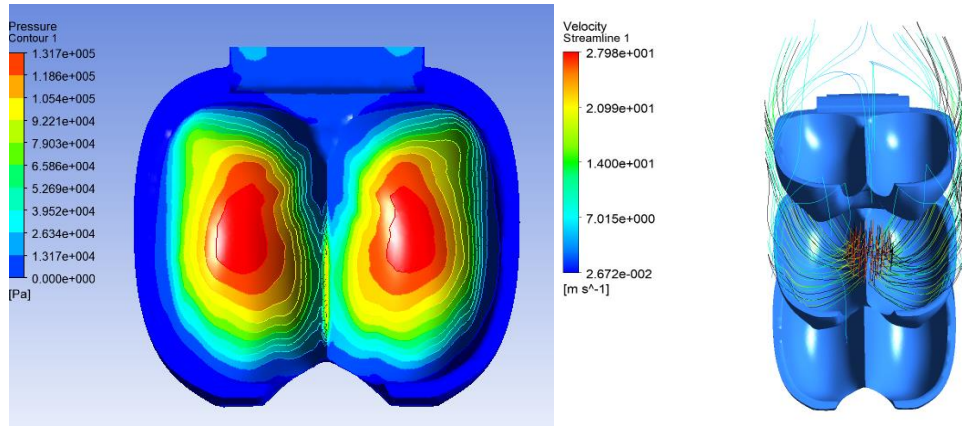
a)   Pressure distribution   b) Particle track

Figure 8. Pressure distribution and Particle tracks

The main objective of this study was to predict the sediment erosion pattern on the Pelton turbine bucket. Tabakoff and Grant model was used for prediction sediment erosion, and erosion was expressed in erosion rate density in the post-processor. With the completion of the CFD simulation, the erosion prediction results can be obtained. Figure 9 (a) and (b) show the erosion distribution in the bucket. It was found that four possible erosion regions were detected which are at the splitter, at the inside area of bucket and backside of the bucket. Also the main possible region of erosion at the tip of the bucket. The value of erosion rate density is directly related to the flow rate of water and the value of particle content in the water.
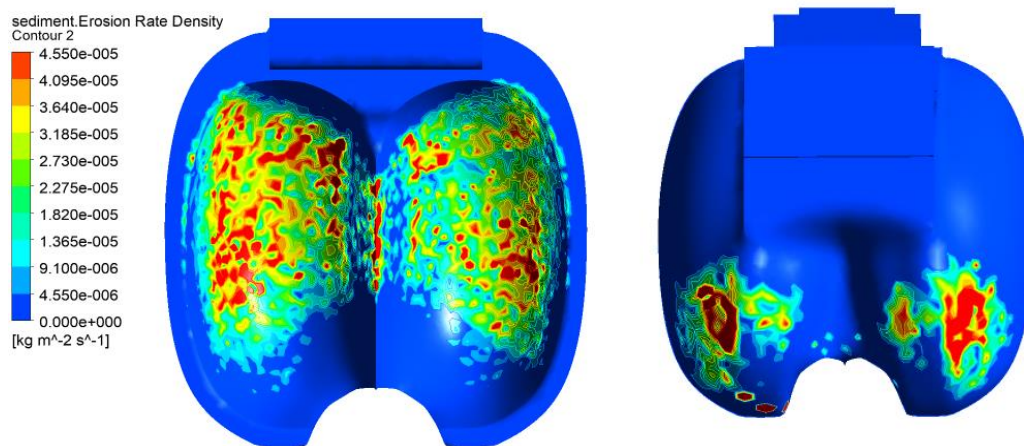


a) Bucket   b) Backside of bucket

Figure 9: Predicted erosion of needle and nozzle

b)   Erosion rate calculation

From experiment erosion rate at a flow rate of 0.004 m^3/s and particle concentration of 261 ppm with the continuous 72 operating hour's 69 mg mass loss in each bucket was found. To compare the mass loss from the simulation result three erosion prone area in the bucket as shown in figure 10 were taken into account. The total accounted area is 7 mm^2 and the calculated value of eroded mass is around 82.5mg.
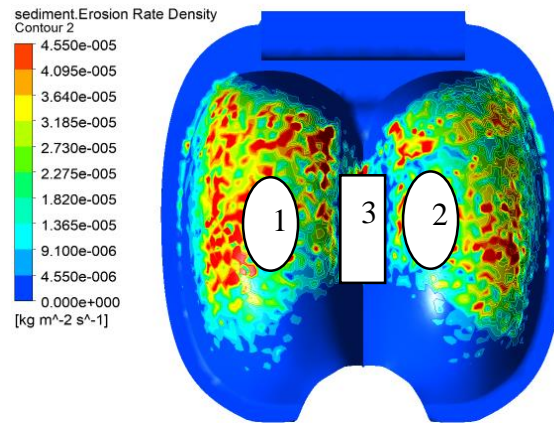
Figure 10. Accounted eroded area

V.   CONCLUSION

The CFD analysis of the micro Pelton turbine of 2 kW design power was performed using ANSYS CFX software to investigate the sediment erosion on the Pelton turbine bucket. Only three buckets were selected to reduce the time and cost in CFD analysis. Tabakoff and Grant model was used and erosion was expressed in erosion rate density in the post-processor. It was found that maximum effect due to sediment in the area of splitter and inside of the bucket. The backside of the bucket is also erosion-prone area. From numerical analysis mass loss due to sediment particle was found 82 mg and deviation from the experimental value is below 20 %. Numerical analysis using CFD can reduce the time and cost to predict the model behavior in a real environment it can be best the option to minimize the dependency in the experimental analysis which is highly time-consuming and costly.

VI.   REFERENCES

[1]   H. P. Neopane, "Sediment Erosion in HydroTurbines, Phd.Thesis " 2010

[2]   T. Bajracharya, B. Acharya, C. Joshi, R. Saini and O. Dahlhaug, "Sand Erosion of Pelton Turbine Nozzles and Buckets: A Case Study of Chilime Hydropower Plant," Wear, vol. 264, no. 3-4, pp. 117-184, 2008.

[3]   R. S. M.K. Padhy, "Effect of size and concentration of silt particles on erosion of pelton turbine bucket," energy, p. 1477–1483, 2009.

[4]   Thapa, B., and H. Brekke. "Effect of sand particle size and surface curvature in erosion of hydraulic turbine." IAHR symposium on hydraulic machinery and systems, Stockholm. 2004

[5]   B. Thapa, "Sand erosion in hydraulic machinery, Phd. Thesis," 2004.

[6]   Saini RP. and Padhy MK., "Study of silt erosion on performance of a Pelton turbine", Energy 36:141-147, 2011

[7]   L. F. Barstad, "CFD Analysis of a Pelton Turbine, Master's Thesis," *NTNU open,* 2012.

[8]   ANSYS CFX Release 14.0, Solver Theory Guide, 2011

[9]   A. Panthee, B. Thapa and H. P. Neopane, "CFD Analysis of Pelton runner," International Journal of Scientific and Research Publications (IJSRP), vol. 4, no.

[10]   Z. Zhang, "Working Principle of Pelton Turbines," in Pelton Turbine, Springer, 2016, pp. 13-40.

[11]   L. F. Barstad, "CFD Analysis of a Pelton Turbine," NTNU open , 2013.

[12]   A. Perrig. F. Avellan, j. L. Kueny, M. Farhat, E. Parkinson, Flow in Pelton Turbine Bucket: Numerical and Experimental Investigations, Transactions of the ASME 128 (2006).